[AMERICAN JOURNAL OF SCIENCE, VOL. 281, JUNE, 1981, P. 697-734]

AN EXPERIMENTAL STUDY OF HORNBLENDE STABILITY AND COMPOSITIONAL VARIABILITY IN AMPHIBOLITE

FRANK S. SPEAR*

Department of Earth and Space Sciences,
University of California, Los Angeles, California 90024

ABSTRACT. The stability of hornblende in a rock of olivine tholeiite composition has been determined under conditions of $P_{fluid} = P_{total}$ on the wüstite–magnetite (WM), quartz–fayalite–magnetite (QFM), and hematite–magnetite (HM) buffers. The assemblage Ca-amphibole + plagioclase + ilmenite is stable under all conditions studied, where oxygen fugacities are defined by the WM and QFM buffers except at the highest temperatures. With increasing temperature, amphibole begins to break down to produce coexisting clinopyroxene, then at successively higher temperatures, clinopyroxene + orthopyroxene and finally clinopyroxene + orthopyroxene + olivine; proportions of the Ca-amphibole gradually diminish over this interval. The temperature for the first appearance of clinopyroxene is 768 ± 8°C, 1.0 kb and 788 ± 8°C kb (f_{O_2} = QFM). Orthopyroxene appears as a breakdown product of amphibole approx 10° to 30°C higher than the first appearance of clinopyroxene, and olivine joins the breakdown assemblage approx 10° to 30°C higher than the first appearance of orthopyroxene. Between the QFM and HM buffers, ilmenite is replaced by titanohematite, the proportion of amphibole decreases, and the proportion of plagioclase + Fe–Ti oxides increases. Along the HM buffer, amphibole breaks down to clinopyroxene only, at temperatures of 695 ± 10°C, 0.5 kb, 720 ± 9°C, 1.0 kb, 735 ± 8°C, 2.0 kb and 738 ± 9°C, 3.0 kb. The upper thermal stability limit of amphibole is determined to be 902 ± 7°, 912 ± 9°, and 908 ± 9°C, 1.0 kb on the HM, QFM, and WM buffers, respectively.

Below the temperature of the first appearance of pyroxene, amphibole coexists with plagioclase + ilmenite ± sphene with f_{O_2} defined by the QFM and WM buffers, and plagioclase + titanohematite ± sphene ± quartz with f_{O_2} defined by the HM buffer. The presence of sphene in the equilibrium assemblage is favored by high P_{fluid} and high f_{O_2}.

Calcic amphiboles synthesized from the olivine tholeiite under subsolidus hydrothermal conditions display systematic changes in composition with T, P_f, and f_{O_2} of formation. At constant P_f and on a given oxygen fugacity buffer, amphiboles are enriched in Na, K, Ti, and Al and depleted in Si with increasing temperature. The same trend occurs at constant T and P_f with decreasing f_{O_2}. In addition, Fe^{3+}/Fe^{2+} (determined by Mössbauer spectroscopy of experimental charges) and Mg/Fe increase in the amphibole with increasing f_{O_2}. On a given oxygen fugacity buffer and at constant T, Al(VI) and Al_{total} increase, whereas Si decreases with increasing P_f.

Amphibole compositional variability may be described in terms of the pargasite, Ti–tschermakite, Fe^{3+}–tschermakite, and glaucophane substitution mechanisms in addition to Fe:Mg exchange. As a group, the amphiboles display an approximately linear trend on a plot of A site occupancy versus Al(IV), with the amount of pargasite substitution increasing with increasing temperature and decreasing f_{O_2} of formation.

Clinopyroxene has an Fe^{2+}/Mg lower than that of coexisting amphibole, whereas coexisting orthopyroxene has a higher Fe^{2+}/Mg; Fe^{3+}/Fe^{2+} in clinopyroxene also increases with f_{O_2} of formation. The composition of ilmenite–hematite solid solutions is relatively insensitive to temperature of synthesis but is very dependent on f_{O_2}, the composition ranging from 0.9 $FeTiO_3$ component on the QFM buffer to 0.25 on the HM buffer. Coexisting plagioclase ranges from An_{42}-An_{58} and displays no systematic trend over the temperature interval 600° to 850°C.

Calculations for $P_{H_2O} < P_{total}$ reveal that the minimum T for the first appearance of pyroxene in this system can be achieved at 700°C by dilution of H_2O to a mole fraction of approx 0.5; complete dehydration of amphibole should occur at this temperature where $X_{H_2O} \cong 0.06$.

* Present Address: Department of Earth and Planetary Sciences, Massachusetts Institute of Technology, Cambridge, Massachusetts 02139

INTRODUCTION

Studies of naturally occurring amphibolites have led to the conclusion that hornblende undergoes changes in composition with increasing metamorphic grade (for example, Engel and Engel, 1962b; Binns, 1965a, b; Leake, 1965; Cooper and Lovering, 1970; Ernst, 1972; Laird, ms). Amphiboles from the greenschist facies are typically actinolitic in composition, whereas Al and Na-rich pargasites are found in the amphibolite and granulite facies. In natural samples, however, the effects of bulk rock chemistry are difficult to distinguish from changes in intensive parameters of metamorphism. Thus, the relationship between hornblende composition and metamorphic grade is, at present, understood only qualitatively, and estimates of metamorphic conditions based on assemblages found in hornblende bearing amphibolites and granulites contain large uncertainties.

This study was undertaken in order to verify experimentally the compositional trends for amphibole in a rock of a single bulk composition and to calibrate experimentally the upper thermal stability of hornblende in a "typical" amphibolite. A mid-ocean ridge olivine tholeiite was chosen as a starting material, because this bulk composition is representative of large volumes of amphibolites and because the study of a natural sample avoids the problem of extrapolating from simple to complex systems. The first part of this report is a discussion of the chemical variability with T, P, and f_{O_2} of hornblende, clinopyroxene, orthopyroxene, plagioclase, and Fe–Ti oxides synthesized from this

TABLE 1

Chemical analyses (wt percent) and molecular norms of V25-RD1-T2

	1		2	3	4
SiO_2	49.43	Qtz	—	—	0.72
TiO_2	1.62	Or	1.10	1.10	1.10
Al_2O_3	15.97	Ab	25.95	25.95	25.95
Fe_2O_3	2.09	An	30.18	30.18	30.18
FeO	7.55	Cp	17.76	17.76	8.88
MnO	0.18	Hy	8.02	13.44	24.98
MgO	8.50	Ol	14.28	6.15	—
CaO	10.73	Mt	—	2.17	5.49
Na_2O	2.87	Il	2.24	2.24	2.24
K_2O	0.18	Ap	0.29	0.29	0.29
P_2O_5	0.15	SUM	99.46	99.82	99.83
Total	99.27				
$\frac{FeO^*}{FeO^*MgO}$	.526	$\frac{Fe^{2+}+Fe^{3+}}{Fe^{2+}+Fe^{3+}+Mg}$	0.38	0.38	0.38
		$\frac{Fe^{2+}}{Fe^{2+}+Mg}$	0.38	0.23	0.06

1. V25-RD1-T2 wt percent oxides (Analyst F. Shido)
2. $Fe^{3+}/Fe^{2+} = 0.0$
3. $Fe^{3+}/Fe^{2+} = 0.25$ (per analysis of original rock)
4. $Fe^{3+}/Fe^{2+} = 1.0$

olivine tholeiite. The second part is a discussion of the subsolidus phase equilibria of this rock.

Liou, Kuniyoshi, and Ito (1974) experimentally investigated the greenschist to amphibolite facies transition and presented compositional data on hornblende and coexisting plagioclase. Binns (1968) presented data on the breakdown of hornblende to orthopyroxene + clinopyroxene but did not analyze the coexisting phases. The present study, in conjunction with these previous studies, should provide an adequate basis for the interpretation of the metamorphic conditions of the amphibolite and granulite facies.

EXPERIMENTAL PROCEDURES

Equipment and techniques.—Cold seal hydrothermal apparatus (Tuttle, 1949) utilizing horizontal pressure vessels and H_2O as a pressure medium was used for all experiments of this study. Experimental charges were run in $Ag_{70}Pd_{30}$ and $Ag_{80}Pd_{20}$ capsules (3.0 mm o.d.). Three different crystalline buffers (Eugster and Wones, 1962) were used to control oxygen fugacity: wüstite–magnetite (WM), quartz–fayalite–magnetite (QFM), and hematite–magnetite (HM). The experimental charges and buffer assemblages were contained in Ag or Au capsules (5.6 mm o.d.).

Temperatures were measured on a Leeds and Northrup K-3 potentiometer using chromel–alumel thermocouples calibrated at 1 atm against the melting of NaCl. Total temperature uncertainty, including thermal gradients, temperature variations, and calibration uncertainties, is believed to be within ± 7°C for all runs and ± 5°C for the majority of runs. Pressure measurements were calibrated against Heise bourdon tube gauges and are believed to be accurate to within ± 50 bars of the specified value.

Starting material.—The starting material used in this study is an olivine tholeiite dredged from the Mid-Atlantic ridge.[1] The rock is crystalline and is composed of approx 10 modal percent olivine phenocrysts (Fo_{85}), set in a groundmass of acicular plagioclase (An_{62}), clinopyroxene, and ilmenite. A chemical analysis and molecular norm for T2 are presented in table 1. Inasmuch as the experiments of the present study utilize conditions of controlled f_{O_2}, which will alter the bulk Fe^{3+}/Fe^{2+} of the rock, it is important to note that at low values of Fe^{3+}/Fe^{2+}, T2 is olivine normative, whereas for Fe^{3+}/Fe^{2+} greater than approx 0.9, T2 becomes quartz normative.

The rock was crushed in a tungsten-carbide ball mill, then ground under acetone in an agate mortar, and dried thoroughly. Distilled H_2O was used as fluid medium, and all experiments were conducted with $P_{fluid} = P_{total}$.

Description of experiments.—Synthesis experiments (using basalt as starting material) and reversal experiments (using previously synthesized amphibolite as starting material) were both performed in this study. The

[1] Specimen V25-RD1-T2 (abbreviated T2 in this study), supplied to the author by A. Miyashiro. Specimen locality described in Miyashiro, Shido, and Ewing (1969).

synthesis experiments were primarily used to monitor phase changes and chemical changes in the amphiboles as a function of time. The reversal experiments were used to define the equilibrium reaction boundaries. All the expreiments were run at conditions below the solidus curve; no melt was observed in any of the run products. The experimental run data are presented in appendix A. An expandable lattice clay mineral, which has been identified as smectite, appeared in many runs below 550°C. A detailed description and the petrologic significance of this phase are given in appendix B.

Electron microprobe technique.—Electron microprobe analyses of the fine grained (1-10μm), experimentally synthesized phases were made using the technique for the analysis of microparticles described first by White (1964) and successfully employed by Eugster and others (1972) and Ferry and Spear (1978). The grains to be analyzed were disaggregated by grinding in a mortar and agitating in an ultrasonic cleaner, then dispersed on a polished industrial diamond and carbon coated. An accelerating potential of 15 kv and sample currents of 40 to 70 nA with a slightly defocused beam were used. Counts were collected for three elements simultaneously, and the counting rates of two elements were normalized to the counting rate of the third element (usually Si). The count ratios were compared to the count ratios of standards to yield weight ratios, and the weight ratios were then normalized to 100 percent for pyroxenes, feldspars, and Fe–Ti oxides and 98 percent for amphiboles.

The assumption inherent in this procedure is that the ratio of X-ray intensity for two elements (for example Mg/Si) is independent of sample size and geometry. Armstrong and Buseck (1975) have shown on theoretical grounds that this is not the case for microparticles in the size

TABLE 2

Comparison of conventional electron microprobe analysis with particulate analysis of two natural amphiboles

	Kaersutite		Hornblende	
	Conventional	Particulate	Conventional	Particulate
SiO_2	39.6(6)*	39.3(11)	46.3(6)	45.1(9)
Al_2O_3	13.5(4)	13.6(6)	10.8(2)	11.1(4)
TiO_2	4.9(1)	4.4(4)	1.4(1)	1.4(1)
FeO	14.3(4)	15.2(13)	14.6(4)	15.3(10)
MgO	10.1(3)	10.1(8)	11.1(3)	10.7(6)
MnO	0.3(1)	0.2(2)	0.3(1)	0.3(1)
CaO	10.9(3)	10.9(12)	11.6(3)	12.2(7)
Na_2O	2.6(1)	2.5(5)	1.6(1)	1.4(2)
K_2O	1.6(1)	1.6(1)	0.9(1)	1.0(1)
Total	97.8	97.8**	98.6	98.6***

* Error is one standard deviation of the mean of 15 to 20 analyses. To be read as 39.3(11) = 39.3 ± 1.1. Error on conventional analysis approx ± 5 percent of amount present for minor elements, ± 3 percent of amount present for major elements.

** Analysis normalized to 97.8.

*** Analysis normalized to 98.6.

range 1 to 10 μm, although in practice, the procedure works well with particles of limited range in size and shape. Table 2 is a comparison of conventional microprobe analyses (that is, analysis of a flat, polished surface) with particulate analyses of two amphiboles. Care was taken to analyze only grains in the 3 to 8 μm size range, although no discrimination was made on the basis of sample geometry. The errors associated with the particulate analyses represent one standard deviation of the distribution of 15 to 20 analyses of separate grains. The results in the table demonstrate that the reproducibility of the particulate analyses is generally within $\pm$ 5 percent of the amount present and that the particulate analyses agree with the conventional analyses generally to within $\pm$ 6 percent of the amount present for major elements. The discrepancies that do exist are thought to be due to the lack of absorption and fluorescence corrections on the particulate analyses and will not affect the trends observed, only the absolute magnitude of the values.

Each analysis in table 3, which contains analyses of the experimental run products, represents the average of between 5 to 20 grains analyzed from the same run product. Errors associated with the oxide weight percents represent one standard deviation of the distribution of these (5-20) analyses.

Ferric iron in the amphiboles.—The $Fe^{3+}/(Fe^{3+} + Fe^{2+})$ in the amphiboles was measured directly on the products of three experiments run at different f_{O_2} buffers but at the same T (700°C) using Mössbauer spectroscopy[2]. The spectra were complicated by the presence of an additional phase — ilmenite in the WM- (T2-130A) and QFM- (T2-61A) buffered experiments and hematite in the HM-buffered (T2-125A + T2-124A) experiment — but peaks due to these phases were resolved, and their effect subtracted from the amphibole spectra. The measured ferric iron proportions of amphiboles synthesized on the WM, QFM, and HM buffers are 11.4 $\pm$ 1.0 percent, 12.5 $\pm$ 1.2 percent, and 40.0 $\pm$ 4.0 percent of the total Fe, respectively. These ferric iron contents were used in the recalculation of all analyses of amphiboles synthesized at the respective buffer.

It is of interest to compare the measured $Fe^{3+}/(Fe^{3+} + Fe^{2+})$ in the amphiboles with the ferric iron content calculated using different procedures described in the literature. The method proposed by Stout (1972), based on stoichiometric constraints, places the following lower and upper limits on the percent of ferric iron: 0.0 to 98.1 percent, 0.0 to 77.1 percent, and 0.0 to 100.0 percent of the total Fe for the amphiboles synthesized on the WM, QFM, and HM buffers, respectively. In each case the calculated ferric iron content brackets the measured ferric iron content; however, the brackets are so broad that the important difference in ferric iron content between amphiboles equilibrated at the QFM and WM buffers and that of amphiboles equilibrated on the HM buffer is obscured. Normalizing the amphibole analyses such that 0.3 Al(IV) = A site occupancy (justification for this procedure is given in Robinson, Ross, and Jaffe,

[2] Mössbauer spectra were collected at the Geophysical Laboratory, Carnegie Institution of Washington, with the assistance of F. Huggins and D. Virgo.

TABLE 3

Electron microprobe analyses of synthetic amphiboles and coexisting plagioclase and Fe–Ti oxides

Run #	T2-119A	T2-124A	T2-45B	T2-84A	T2-80B	T2-57A	T2-81A	T2-58A	T2-126A	T2-102A
Buffer	HM	HM	HM	HM	QFM	QFM	QFM	QFM	QFM	QFM
P Kb	1.0	1.0	1.0	1.0	1.0	1.0	1.0	1.0	1.0	1.0
T°C	650	706	754	883	599	651	707	750	802	850
Time(hrs)	843	574	695	169	3059	1202	574	1770	248	241
					Weight % oxides					
SiO_2	52.3(6)†	52.0(11)	52.3(19)	49.7(9)	49.3(5)	48.9(8)	49.2(13)	48.8(11)	46.6(20)	46.7(14)
Al_2O_3	6.2(12)	5.5(6)	6.1(5)	8.5(3)	6.6(8)	7.3(6)	7.7(6)	7.8(7)	9.0(13)	9.7(8)
TiO_2	0.4(2)	0.5(1)	0.5(1)	1.4(2)	0.8(5)	0.7(1)	1.1(1)	1.4(1)	1.8(2)	2.2(2)
MgO	19.0(8)	20.9(8)	20.8(10)	19.5(11)	14.5(5)	15.1(6)	14.0(9)	13.9(8)	13.8(11)	12.6(8)
FeO	7.3(20)	6.9(5)	7.2(4)	6.5(5)	16.9(2)	14.9(10)	14.7(11)	14.2(9)	13.9(15)	13.7(7)
MnO	0.2(2)	0.5(1)	0.4(1)	0.5(1)	0.2(1)	0.2(1)	0.2(1)	0.3(1)	0.3(1)	0.2(1)
CaO	11.3(21)	10.6(9)	9.4(7)	9.3(5)	9.1(5)	9.1(4)	9.1(6)	9.7(7)	10.4(10)	10.3(6)
Na_2O	1.2(3)	1.0(3)	1.2(2)	2.3(3)	1.4(4)	1.6(2)	1.9(3)	1.8(3)	2.0(5)	2.2(2)
K_2O	0.1(1)	0.1(1)	0.1(0)	0.3(1)	0.0(0)	0.1(0)	0.1(1)	0.1(1)	0.2(1)	0.3(1)
Total*	98.00	98.0	98.0	98.0	98.0	98.0	98.0	98.0	98.0	98.0
					Cations per 23 oxygens					
Si	7.27	7.23	7.25	6.93	7.15	7.07	7.10	7.04	6.77	6.78
Al(IV)	0.73	0.77	0.75	1.07	0.85	0.93	0.90	0.96	1.23	1.22
Al(VI)	0.29	0.14	0.25	0.33	0.28	0.32	0.42	0.37	0.32	0.45
Ti	0.04	0.05	0.05	0.15	0.09	0.08	0.12	0.15	0.20	0.24
Fe^{3+}**	0.34	0.32	0.33	0.30	0.23	0.22	0.21	0.21	0.20	0.20
Mg	3.94	4.34	4.29	4.05	3.13	3.25	3.01	3.00	2.99	2.74
Fe^{2+}	0.51	0.48	0.50	0.46	1.71	1.59	1.56	1.50	1.49	1.46
Mn	0.03	0.06	0.05	0.05	0.03	0.02	0.03	0.03	0.03	0.02
Ca	1.68	1.58	1.40	1.39	1.42	1.41	1.41	1.51	1.62	1.61
Na(M4)	0.17	0.04	0.14	0.26	0.12	0.22	0.25	0.23	0.15	0.29
Na (A)	0.16	0.22	0.18	0.35	0.28	0.34	0.27	0.28	0.41	0.32
K	0.02	0.02	0.02	0.05	0.03	0.01	0.02	0.03	0.04	0.05
Sum	15.18	15.24	15.20	15.39	15.38	15.35	15.29	15.31	15.45	15.37
An%***	49	50	44	42	50	--	--	49	58	47
n_1††	--	1.655	1.657	1.665	--	--	1.670	1.674	--	1.682
nβ	--	1.636	1.640	1.650	--	--	1.650	1.655	--	1.667
nα	--	1.632	1.637	1.646	--	--	1.643	1.650	--	1.664
X_{FeTiO_3}†††	0.22	0.28	0.21	0.24	0.50	--	--	--	0.93	0.94

Run #	T2-42A	T2-41B	T2-43B	T2-125A	T2-44A	T2-56	T2-62A	T2-55A	T2-61A	T2-54A	T2-126A	T2-77A
Buffer	HM	HM	HM	HM	HM	QFM	QFM	QFM	QFM	QFM	HM	QFM
P Kb	3.0	3.0	3.0	3.0	3.0	3.0	3.0	3.0	3.0	3.0	5.0	5.0
T°C	550	605	642	701	752	551	610	655	699	763	698	710
Time(hrs)	1315	1164	1379	628	263	1683	1944	1140	1049	1243	534	471
						Weight % oxides						
SiO_2	54.5(12)	54.5(5)	52.7(5)	51.3(9)	50.4(19)	51.2(12)	51.0(9)	49.8(11)	48.8(9)	47.8(8)	49.2(9)	48.0(5)
Al_2O_3	5.2(3)	5.8(3)	6.3(7)	6.7(5)	7.3(13)	5.2(7)	5.7(6)	7.2(5)	8.1(5)	8.3(5)	8.8(5)	9.1(9)
TiO_2	0.2(1)	0.4(2)	0.6(2)	0.5(3)	0.6(1)	0.5(1)	0.5(1)	0.8(1)	1.0(2)	1.4(2)	1.7(1)	1.1(2)
MgO	18.6(3)	18.0(13)	18.0(6)	18.3(9)	17.6(16)	12.6(16)	13.2(6)	13.3(6)	13.2(2)	13.4(2)	13.0(6)	13.9(9)
FeO	7.9(14)	8.0(11)	7.9(4)	7.8(5)	8.6(2)	14.0(13)	12.5(7)	15.1(10)	14.7(6)	14.6(6)	14.5(5)	13.5(5)
MnO	0.4(3)	0.5(2)	0.4(1)	0.4(1)	0.4(1)	0.4(1)	0.3(1)	0.3(1)	0.3(1)	0.3(1)	0.4(1)	0.2(1)
CaO	10.3(5)	10.1(6)	10.8(9)	10.9(6)	11.0(6)	9.2(15)	8.9(2)	9.5(7)	9.3(2)	10.1(6)	10.8(8)	10.0(6)
Na_2O	0.7(2)	1.0(3)	1.1(2)	1.4(1)	1.6(3)	0.7(3)	1.0(2)	1.4(3)	1.9(2)	1.9(2)	1.5(1)	1.9(2)
K_2O	0.1(1)	0.1(1)	0.1(0)	0.2(0)	0.1(0)	0.1(1)	0.1(1)	0.1(1)	0.2(0)	0.2(1)	0.2(1)	0.1(0)
Total*	98.0	98.0	98.0	98.0	98.0	98.0	98.0	98.0	98.0	98.0	98.0	98.0
						Cations per 23 oxygens						
Si	7.53	7.53	7.33	7.15	7.01	7.24	7.30	7.20	7.05	6.95	6.91	6.92
Al(IV)	0.47	0.47	0.67	0.85	0.99	0.76	0.70	0.80	0.95	1.05	1.09	1.08
Al(VI)	0.39	0.44	0.37	0.25	0.38	0.11	0.27	0.43	0.47	0.47	0.39	0.50
Ti	0.02	0.04	0.06	0.05	0.07	0.05	0.06	0.09	0.11	0.15	0.08	0.12
Fe^{3+}**	0.37	0.37	0.32	0.36	0.36	0.26	0.26	0.22	0.21	0.21	0.22	0.20
Mg	3.84	3.71	3.73	3.60	3.48	2.79	2.82	2.87	2.95	2.90	2.58	2.99
Fe^{2+}	0.55	0.55	0.55	0.55	0.56	1.92	1.87	1.60	1.56	1.59	0.66	1.44
Mn	0.05	0.06	0.04	0.04	0.05	0.05	0.04	0.04	0.04	0.04	0.05	0.02
Ca	1.53	1.50	1.60	1.63	1.65	1.43	1.37	1.51	1.43	1.57	1.62	1.54
Na(M4)	0.19	0.27	0.26	0.17	0.23	0.19	0.21	0.25	0.24	0.19	0.18	0.20
Na(A)	0.00	0.00	0.41	0.30	0.21	0.03	0.06	0.21	0.28	0.33	0.24	0.34
K	0.02	0.01	0.02	0.03	0.03	0.01	0.01	0.02	0.02	0.01	0.03	0.02
Sum	14.96	14.99	15.43	15.23	15.23	15.04	15.07	15.23	15.40	15.36	15.23	15.35
An%***	--	--	--	50	52	--	--	48	46	56	44	48
n_1††	--	--	--	--	--	--	--	--	--	--	1.669	1.667
nβ	--	--	--	--	--	--	--	--	--	--	1.645	1.652
nα	--	--	--	--	--	--	--	--	--	--	1.640	1.646
X_{FeTiO_3}†††	--	--	--	--	--	--	--	--	--	--	0.26	0.46

* Totals are normalized to 98.0.

** $Fe^{3+}/Fe^{3+}+Fe^{2+}$ determined by Mossbauer spectroscopy to be 0.40 on HM buffer and 0.12 on QFM buffer.

† Numbers in parentheses are one standard deviation of last significant digits. For example, 52.0(11) means 52.0 ± 1.1.

†† Refractive indices of amphiboles measured to ± 0.004.

*** Composition of plagioclase from experiments.

††† Composition of ilmenite from experiments.

1971) yields ferric iron contents of 13.5, 13.3, and 47.7 percent of the total iron for the three amphiboles synthesized at the WM, QFM, and HM buffers respectively. These numbers are close to the measured values and provide a reasonable estimate of the observed ferric iron content.

Recalculation of amphibole analyses.—Amphibole analyses were recalculated on an anhydrous basis assuming 23 oxygens per half unit cell and the Fe^{3+}/Fe^{2+} values given above and assigned to structural positions as follows:

1. Tetrahedral site: all Si, then sufficient Al to sum to 8.0.
2. M1-M2-M3 sites: remaining Al, then Ti, Fe^{3+}, Mg, Fe^{2+}, and Mn to sum to 5.0.
3. M4 site: Ca first, then remaining Fe^{2+}, Mn, and sufficient Na to sum to 2.0.
4. A site: remaining Na and K.

This procedure is identical to that used by Czamanske and Wones (1973) and can be defended on the basis of crystal chemical considerations (Papike, Ross, and Clarke, 1969). Results of the recalculations are included in table 3. It is important to note that although the analyses reported in weight percent are normalized to 98.0 percent, the cation proportions are independent of this normalization, because they are normalized to balance 23 oxygens or 46 positive charges.

RESULTS: MINERAL CHEMISTRY

Equilibration of amphibole compositions.—Most of the analyses reported in table 3 were made on amphiboles synthesized directly from basalt. To demonstrate the equilibration of these amphiboles, three approaches were attempted. First, amphiboles synthesized initially at 763°C, P_f = 3 kb, QFM buffer were rerun at 506°C (855 hrs), 561°C (334 hrs), and 607°C (761 hrs). The compositions of the amphiboles produced in these experiments are plotted in figure 3 and labelled "R". As can be seen in the figure, the compositions of these amphiboles approach the composition of amphiboles synthesized directly from basalt, but the reequilibration is very sluggish.

The second approach used to demonstrate equilibrium was to monitor amphibole compositions as a function of duration of synthesis experiment, and the third approach was to oxidize or reduce the amphibole by changing the f_{O_2} of the experiment at constant T and P_f. Results of these experiments are plotted in figure 1. Data from the oxidation and reduction experiments indicate that amphiboles will be oxidized or reduced but that this process is sluggish, even at 750°C. The plot of amphibole composition versus duration of synthesis demonstrates that within 50 hrs at 750°C, the composition of the amphibole synthesized directly from basalt is statistically indistinguishable from the composition of the amphibole after 1200 hrs, with the exception of Ca content, in spite of the fact that the phase assemblage in the 50 hr experiment has not achieved equilibrium as evidenced by the presence of relict clinopyroxene in the resulting assemblage. Calcium achieved the "equilibrium" compo-

sition after 290 hrs. The rapid attainment of the equilibrium composition by these amphiboles is taken as evidence that amphiboles formed directly from basalt grow essentially on the equilibrium composition.

Hornblende Composition as a Function of T, P_{fluid}, and f_{O_2} of Formation

The change in amphibole composition with temperature at constant P_f can be seen in figures 2 (P_f = 1 kb) and 3 (P_f = 3 kb). The cations that display the largest temperature dependence are Al, Na, K, and Ti, which increase with increasing temperature, and Si, which decreases with increasing temperature. The ratio Fe/Mg is relatively insensitive to temperature, although there is some indication that Fe total (and hence Fe/Mg) decreases slightly with increasing temperature at low oxygen fugacities. Ca increases slightly on all buffers with increasing T at P_f = 3 kb (fig. 3); at P_f = 1 kb (fig. 2), Ca decreases in amphiboles on the HM buffer and increases in amphiboles on the QFM buffer.

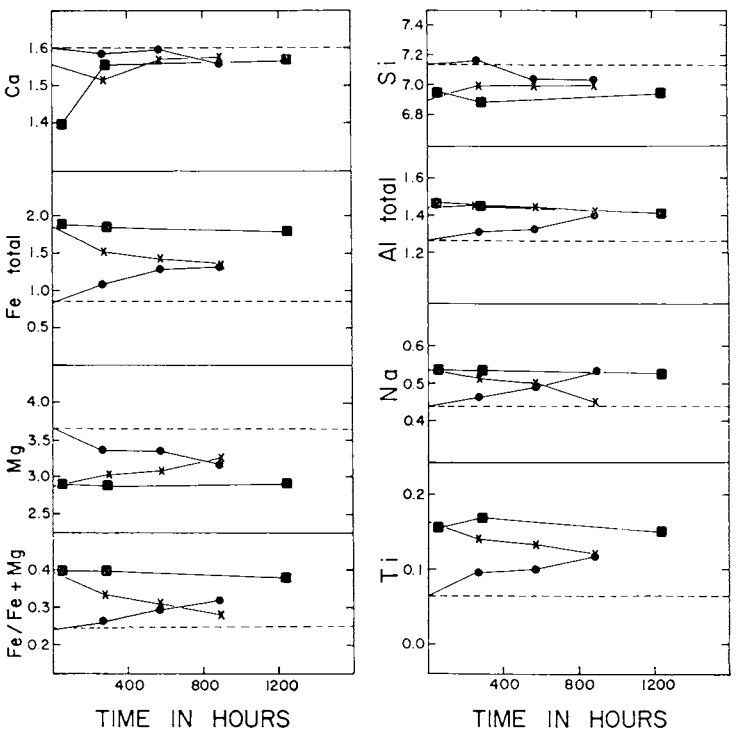

Fig. 1. Amphibole compositions plotted as a function of duration of experiment: T = 750°C; P_f = 3 kb. Symbols are as follows: squares — QFM buffer, starting material = crystalline basalt; circles — QFM buffer, starting material = amphibolite synthesized on the HM buffer; crosses — HM buffer, starting material = amphibolite synthesized on the QFM buffer. The dashed line is the composition of amphiboles synthesized directly from basalt on the HM buffer. Note that the circles approach the squares in composition with increasing time, and the crosses approach the dashed line. Also note that there is very little change in amphibole composition after the first 50 hrs of synthesis (squares).

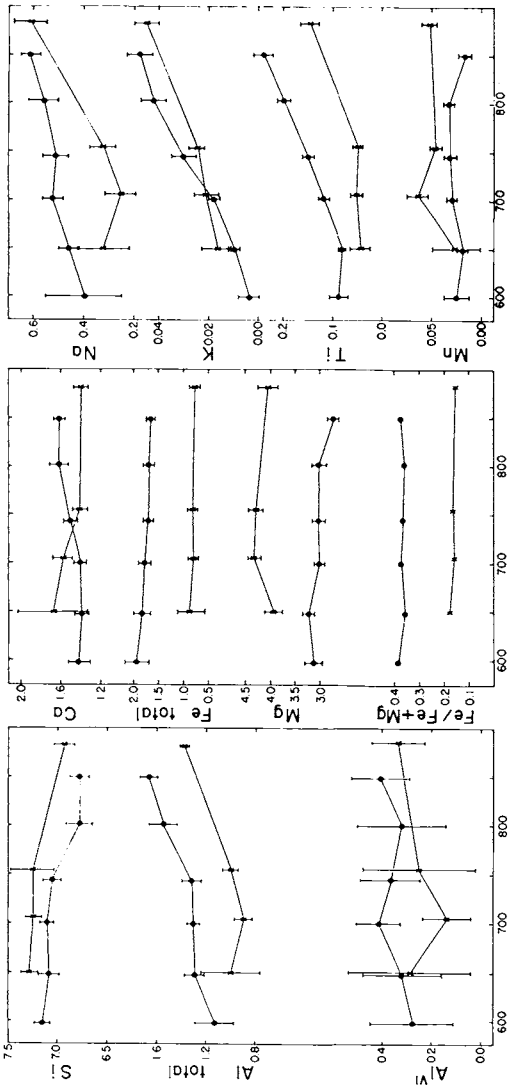

Fig. 2. Cation proportions of amphiboles synthesized directly from basalt plotted as a function of temperature of experiment: $P_f = 1$ kb. Closed circles indicate experiments conducted with oxygen fugacities defined by the QFM buffer, crosses indicate experiments run with oxygen fugacities defined by the HM buffer. Error bars are maximum errors calculated as described in the text.

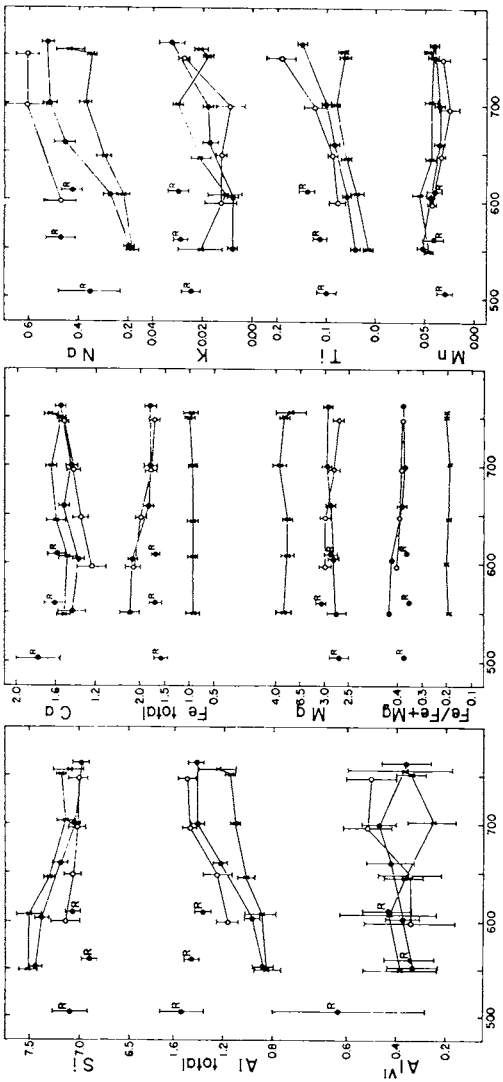

Fig. 3. Cation proportions of amphiboles synthesized directly from basalt plotted as a function of temperature of experiment; $P_t = 3$ kb. Open circles indicate experiments run with f_{O_2} defined by the WM buffer, closed circles indicate experiments run with f_{O_2} defined by the QFM buffer, and crosses indicate experiments run with f_{O_2} defined by the HM buffer. Error bars represent maximum errors calculated as described in text. Points labelled "R" are from experiments made with synthetic amphibolite starting material (starting material synthesized at 763°C, $P_t = 3$ kb, QFM) and run at the indicated temperatures, $P_t = 3$ kb, QFM buffer.

Also apparent in figures 2 and 3 is a systematic shift in composition with oxygen fugacity of formation. In general, Si, Mg, and Mn increase with increasing oxygen fugacity of formation, whereas Al, Fe, Na, K, Ti, and Fe/Mg decrease. The relationship between amphibole composition and oxygen fugacity of formation is also depicted in figure 4, where cation proportions have been plotted against log f_{O_2} at 750°C, P_f = 3 kb. It should be noted that because Fe^{3+}/Fe^{2+} increases with increasing oxygen fugacity, the Fe^{2+} content decreases even more at high oxygen fugacities than is indicated in figure 4, in which Fe total is plotted.

Figure 5 is a plot of amphibole compositions versus P_f at 700°C. The cations that display the largest pressure dependence are Si, which decreases with increasing fluid pressure, and Al total and Al(VI), which increase with increasing fluid pressure. The other cations display trends that appear to depend chiefly on the oxygen fugacity of formation. For example, for amphiboles synthesized on the HM buffer, Mg and Mn decrease with increasing fluid pressure, and Na, Fe total and Fe total/Mg increase. These trends are not observed in the amphiboles synthesized on the WM and QFM buffers.

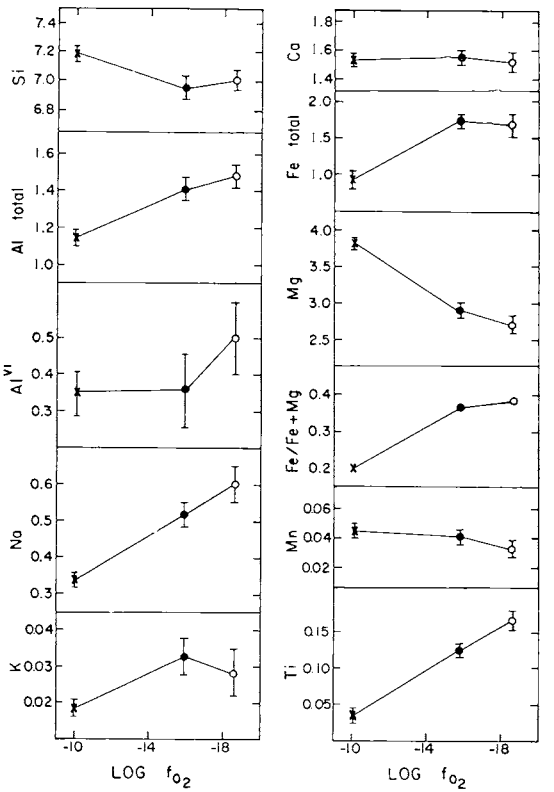

Fig. 4. Cation proportions of amphiboles synthesized directly from basalt plotted against log f_{O_2} of formation; 750°C, P_f = 3 kb. Symbols as in figure 3.

Na(M4) in amphiboles has been taken as an indicator of pressure of metamorphism by many authors (Brown, 1977; Laird, ms; Shido and Miyashiro, 1959). However, a plot of Na(M4) versus pressure (not shown here) is similar in appearance to the plot of total Na versus P (fig. 5): there is a systematic increase in Na(M4) with pressure for amphiboles synthesized on the HM buffer; amphiboles synthesized on the QFM buffer show a slight decrease in Na(M4) with P, and amphiboles synthesized on the WM buffer show a strong decrease in Na(M4) with pressure. The errors on Na(M4) are in most cases larger than the values themselves, and the significance of these results is somewhat dubious. Calibration of Na(M4) as a function of P would be a valuable aid to estimates of metamorphic pressures, but evidently this parameter is a sensitive function of oxidation state and possibly bulk composition.

Discussion.—With regard to the compositional changes in hornblende and plagioclase with metamorphic grade from regionally metamorphosed amphibolites, Leake (1965) concluded: (1) the composition of hornblende in metamorphic rocks is mainly controlled by bulk rock composition; (2) in the presence of a Ti-bearing phase such as rutile, ilmenite, or sphene, the Ti content of hornblende increases with tempera-

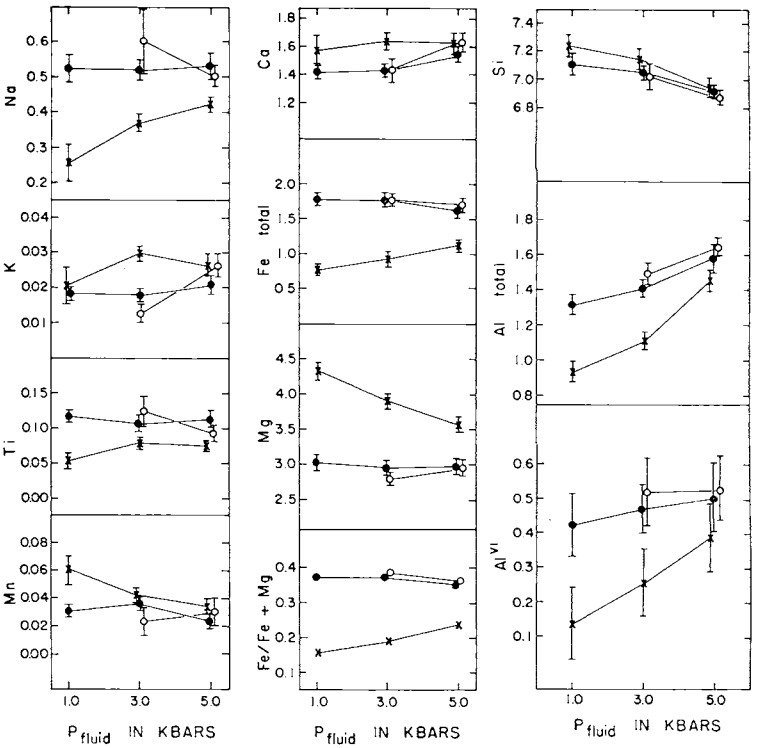

Fig. 5. Cation proportions of amphiboles synthesized directly from basalt plotted against P_f = of formation, 700°C. Symbols as in figure 3.

ture of formation; (3) the amount of Al(VI) in hornblende is apparently related to the pressure of crystallization, but this effect is difficult to quantify inasmuch as the Al(VI) content of the hornblende is also controlled by bulk rock composition; (4) there are systematic changes in the Na/Na + Ca and Al/Si ratios in both hornblende and coexisting plagioclase with increasing grade of metamorphism, although these changes are difficult to distinguish from changes in bulk rock chemistry; and (5) the K, Na, Al(VI), and Al(IV) contents of hornblendes increase with increasing metamorphic grade, whereas Si decreases.

Data from the present study confirm certain compositional trends in amphiboles with changing intensive parameters for an isochemical system. The elements Ti, Na, K, Al_{total}, and Al(IV) all increase with increasing temperature, whereas Si decreases. The most notable compositional changes with increasing fluid pressure include: (1) an increase in Al total; (2) an increase in Al(VI), only notable on the HM buffer; (3) a decrease in Si and sympathetic increase in Al(IV); (4) an increase in Fe, Fe/Mg, and Na and a decrease in Mg, noted only on the HM buffer. Amphibole composition is very strongly dependent on oxygen fugacity with Si, Mg, Mn, and Fe^{3+} increasing and Al_{total}, Al(IV), Na, K, Fe, Ti, and Fe/Mg decreasing with increasing f_{O_2}.

The effect of SiO_2 saturation on amphibole composition.—Amphiboles from two experimental charges run with excess SiO_2 were also analyzed. Experimental conditions were 675°C (T2-Q6) and 725°C (T2-Q7A), 3 kb, QFM buffer. The starting material was a previously synthesized amphibolite, undersaturated with respect to SiO_2, to which quartz was added.

Analyses of the two experiments and of the starting composition of the amphibole (T2-AS5B) are presented in table 4. Sample T2-Q6 has apparently reacted sluggishly but does show minor enrichment in SiO_2 and depletion in Al_2O_3 and Na_2O over the starting material. Comparison of the analysis of T2-Q7A with the analyses of T2-61A and T2-54A clearly demonstrates that the amphibole formed under conditions of excess SiO_2 is more Si-rich and Al- and Na-poor than amphiboles formed under similar conditions without excess SiO_2. In addition, the A site occupancy is also lower in the amphiboles run with excess SiO_2.

These results indicate the importance of bulk SiO_2 content (and therefore silica activity) in determining amphibole chemistry. In general, the effect of higher SiO_2, at constant alkali content, appears to be to shift the composition of the amphibole away from pargasitic (that is, Na- and Al-rich) compositions. This result is to be expected, inasmuch as pargasite and ferropargasite are undersaturated with respect to SiO_2 and should react in the presence of quartz to form a less pargasitic amphibole + other phases by a reaction such as

$$\underset{\text{pargasite}}{2NaCa_2Mg_4AlAl_2Si_6O_{22}(OH)_2} + \underset{\text{quartz}}{8SiO_2} =$$

$$\underset{\text{tremolite}}{Ca_2Mg_5Si_8O_{22}(OH)_2} + \underset{\text{tschermakite}}{Ca_2Mg_3Al_2Al_2Si_6O_{22}(OH)_2} + \underset{\text{albite}}{2NaAlSi_3O_8}.$$

It should also be noted that experiments run on the HM buffer contain free quartz, whereas those run on the QFM and WM buffer do not; accordingly, amphiboles synthesized on the HM buffer are also less pargasitic than those synthesized at lower f_{O_2}.

Substitution Mechanisms in Amphiboles

Compositional variations in amphiboles can be considered in terms of substitutions into the basic tremolite formula, $\square\ Ca_2Mg_5Si_8O_{22}(OH)_2$. These substitutions can either be simple substitutions such as Fe^{2+} or Mn^{2+} for Mg^{2+}, which require no charge balancing, or complex substitutions, which require coupling to maintain charge balance. Coupled substitutions, when carried to an extreme, lead to idealized end-member compositions after which the substitution mechanism is named. Some of the more common coupled substitutions include:

1.	$\square$ (A) + Si(IV)	= Na(A) + Al(IV)	Edenite
2.	2Si(IV) + 2Mg(VI)	= 2Al(IV) + 2Al(VI)	Tschermakite
3.	2Si(IV) + 2Mg(VI)	= 2Al(IV) + $2Fe^{3+}$(VI)	Ferritschermakite

TABLE 4

Electron microprobe analyses of amphiboles from experiments run with excess SiO_2 at 3.0 kb, QFM buffer

Run #	T2-AS5B*	T2-Q7A	T2-Q6
T°C	720	722	675
Duration (hrs.)	432	1329	1720
SiO_2	48.8(10)	50.0(12)	49.8(12)
Al_2O_3	9.3(19)	7.3(5)	7.4(14)
TiO_2	0.9(2)	1.0(1)	0.9(1)
FeO	13.0(9)	14.1(9)	14.3(7)
MgO	14.2(20)	14.0(8)	14.2(7)
MnO	0.1(1)	—	—
CaO	9.9(7)	10.3(6)	10.0(6)
Na_2O	1.5(3)	1.3(1)	1.3(1)
K_2O	0.2(1)	—	—
Total	98.0	98.0	98.0
Si	6.99	7.19	7.16
Al(IV)	1.01	0.81	0.84
Al(VI)	0.56	0.42	0.41
Ti	0.09	0.11	0.10
Fe^{3+}**	0.19	0.20	0.21
Fe^{2+}	1.38	1.49	1.52
Mg	3.05	3.01	3.05
Mn	0.02	—	—
Ca	1.52	1.58	1.55
Na(M4)	0.19	0.19	0.17
Na(A)	0.23	0.16	0.19
K	0.03	—	—
Sum	15.26	15.16	15.19

* Starting composition of the amphiboles.

** $Fe^{3+}/(Fe^{3+} + Fe^{2+})$ assumed to be 0.12.

4. $2Ca(M4) + 2Mg(VI) = 2Na(M4) + 2Al(VI)$ Glaucophane
5. $2Ca(M4) + 2Mg(VI) = 2Na(M4) + 2Fe^{3+}(VI)$ Riebeckite
6. $\square(A) + Ca(M4) = Na(A) + Na(M4)$ Richterite
7. $2Si(IV) + Mg(VI) = 2Al(IV) + Ti(VI)$ Ti–tschermakite
8. $\square(A) + Mg(VI) + 2Si(IV) = Na(A) + Al(VI) + 2Al(IV)$ Pargasite

The symbols in parentheses represent the structural position of the cation, and the symbol □ indicates a vacancy. It should be noted that of these 8 substitution mechanisms, only 5 are algebraically independent. The discussion that follows will be directed at determining which of the possible substitution mechanisms are consistent with the compositional trends observed in the amphiboles synthesized in this study.

A plot of Al(IV) versus A site occupancy (fig. 6) shows a linear relationship with a slope of 2.0. A slope of 1.0 would suggest that substitution (1) was active in determining A site occupancy. A slope of 2.0 indicates that there are 2.0 Al(IV) for every A site cation, consistent with a substitution of type (8) (pargasite). The intercept at approx 0.45 Al(IV) for 0.0 A site cations indicates that all the A site occupancy is compensated for by Al(IV) and that substitution (6) (richterite) is probably not operative. The residual of 0.45 Al(IV) requires additional substitutions involving Al(IV), for example substitutions (2), (3), or (7).

Figure 7A and B are plots of Al(IV) versus Al(VI) and Al(IV) versus Ti, respectively. The tschermakite substitution would require a 1:1 cor-

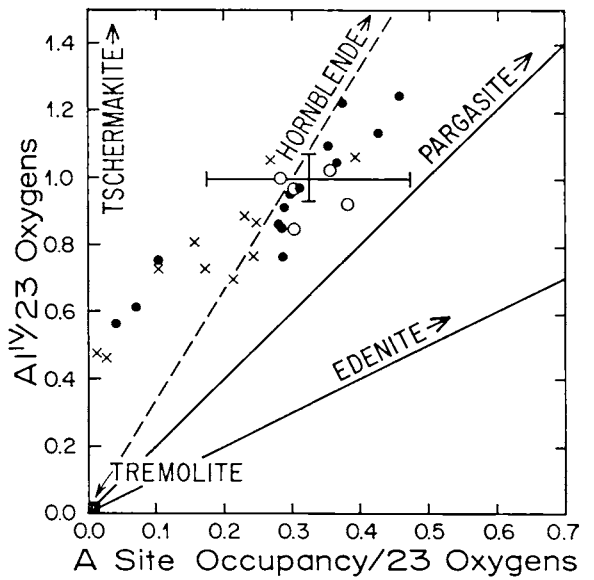

Fig. 6. Plot of Al(IV) versus A site occupancy for amphiboles encountered in this study. Open circles represent amphiboles synthesized on the WM buffer; closed circles, QFM buffer; and crosses, HM buffer. The error bar is the average of errors calculated as described in text. Also indicated are the plotting positions of different amphibole endmembers.

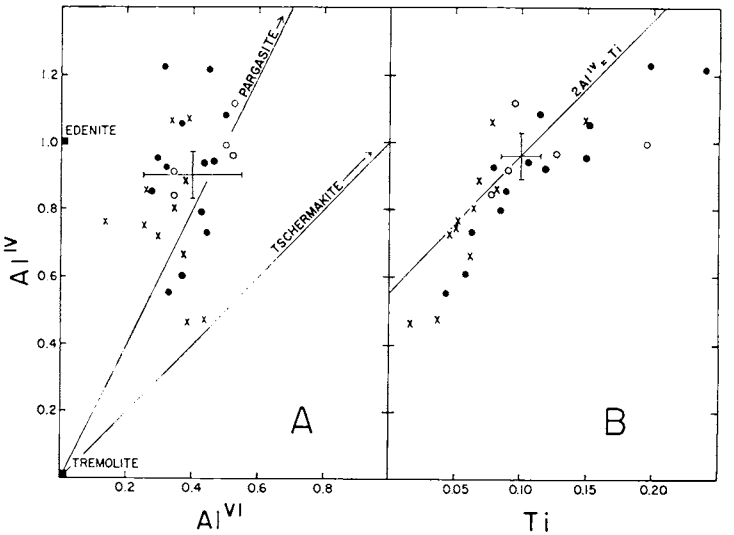

Fig. 7. (A) Plot of Al(IV) versus Al(VI) for amphiboles produced in this study. (B) Plot of Al(IV) versus Ti for amphiboles encountered in this study. Symbols as in figure 6.

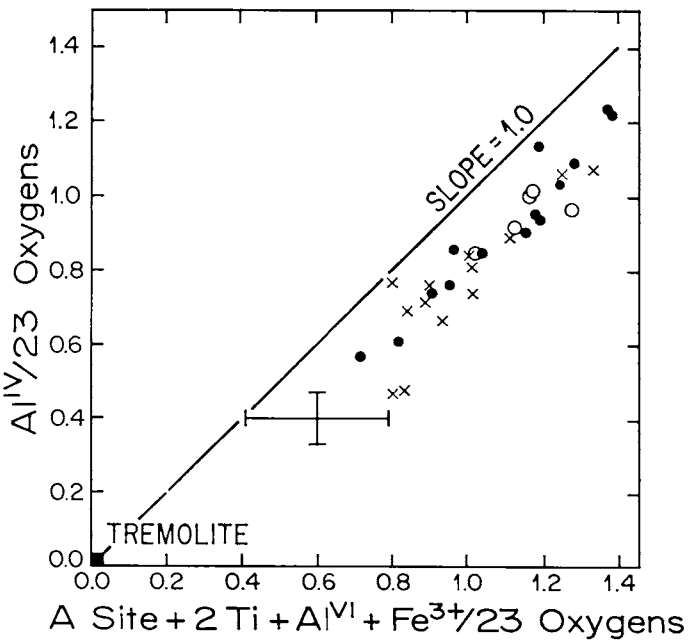

Fig. 8. Plot of Al(IV) versus A site occupancy + 2Ti + Al(VI) + Fe^{3+} for amphiboles encountered in this study. Symbols as in figure 6. Line with a slope of 1.0 is also indicated.

respondence between Al(IV) and Al(VI). It is evident from figure 7A that the relationship is more nearly 2:1. The lack of strong 1:1 correspondence suggests that the tschermakite substitution is not independent but rather coupled with the edenite substitution to produce a pargasite substitution, as previously concluded (fig. 6).

The correlation between Al(IV) and Ti (fig. 7B) is approx 2Al(IV) = Ti, and the intercept on the ordinate at approx 0.55 Al(IV) indicates that all the observed variability in Ti can be accounted for by the Ti–tschermakite substitution. The correlation in figure 7B with a line with a slope of 2.0 indicates that the Ti–tschermakite substitution is independent of other substitutions involving Al(IV).

Substitutions (1), (2), (3), and (7) all involve Al(IV). If all the A site occupancy, Al(VI), Fe^{3+}(VI), and Ti(VI) in the amphibole are coupled to Al(IV), then a plot of Al(IV) versus A site occupancy + 2Ti + Al(VI) + Fe^{3+}(VI) should pass through the origin with a slope of 1.0. Figure 8 is such a plot, and it can be seen that the slope of the data is close to 1.0. The intercept on the abscissa is approx 0.2, however, indicating that some of either the A site cations, Ti, Al(VI), or Fe^{3+} must also be involved in substitutions such as glaucophane, riebeckite, richterite, or a substitution such as 2Na(M4) + Ti(VI) = 2Ca(M4) + Mg(VI). No correlation is observed in plots of Na(M4) versus A site occupancy (fig. 9C) and Na(M4) versus Ti (fig. 9B). Good correlation is observed in a plot of Na(M4) versus Al(VI) (fig. 9A), which indicates that a certain amount of Al (VI) is accountable by the glaucophane substitution.

In summary, the compositional changes in the amphiboles encountered in this study can be described in terms of the pargasite, Ti–tschermakite, and glaucophane substitutions, in addition to simple Fe^{2+} for Mg^{2+} exchange.

Results of Electron Microprobe Analyses on Pyroxenes, Opaque Oxides, and Plagioclase

Pyroxenes.—Pyroxenes were analyzed from two experimental run products, T2-R44 and T2-102A (table 5). T2-R44 contains clinopyroxene and T2-102A contains clinopyroxene + orthopyroxene. Both of the clinopyroxenes are subcalcic augites. There is a strong dependence of Fe^{2+}/Mg in the clinopyroxenes with the oxygen fugacity of formation, similar to the relationship found in the amphiboles. For both experiments, the Fe^{2+}/Mg of the clinopyroxene is smaller than Fe^{2+}/Mg in the amphibole from the same charge with K_D(amp-cpx) = 2.46[3] in the HM buffered experiments and K_D(amp-cpx) = 1.27 in the QFM buffered experiment.

The Fe^{3+}/Fe^{2+} in the clinopyroxenes increases with increasing oxygen fugacity of formation. The ferric iron contents of the clinopyroxenes were determined from stoichiometry and are thus sensitive to analytical error; however, the difference in Fe^{3+} between the clino-

[3] $K_D(A\text{-}B) = (Fe^{2+}/Mg)_A/(Fe^{2+}/Mg)_B$.

pyroxenes from T2-R44 and T2-102A is believed to be too large to be attributed entirely to analytical error.

The orthopyroxene from T2-102A has an Fe^{2+}/Mg larger than both the amphibole and the clinopyroxene from the same run product (K_D(amp-cpx) = 0.58). Hence, where amphibole coexists with orthopyroxene and clinopyroxene, the Fe^{2+}/Mg of the amphibole is intermediate between those of the pyroxenes. This relationship is also observed in natural assemblages (Stoddard, ms; Engel and Engel, 1962b).

Fe–Ti oxides.—Fe–Ti oxides were analyzed on the electron microprobe by taking the ratio of Fe to Ti counts on microparticles, converting to a weight ratio, and then to a molecular ratio. Endmember compositions were calculated using stoichiometry and assuming that the phases consisted of solutions of the endmembers $FeTiO_3$–Fe_2O_3 (for ilmenites and titanohematites) and $FeTi_2O_5$–Fe_2TiO_5 (for pseudobrookites) (table 3).

The ilmenites stable on the QFM buffer range in composition from 0.90 to 0.96 $FeTiO_3$ component, and the titanohematites stable on the HM buffer range in composition from 0.21 to 0.26 $FeTiO_3$ component. The chemical variations within a group may be the result of analytical uncertainties, or they may reflect real variations in composition with temperature and fluid pressure of formation. It is clear, however, that the oxygen fugacity has a much stronger influence on the Fe–Ti oxide composition than either T or P_f.

Plagioclase.—Plagioclase feldspars were analyzed using the same techniques as the amphiboles. A set of working curves was generated using synthetic plagioclase standards of compositions An_{20}, An_{40}, An_{60}, An_{80}, and An_{100}. The ratios Al/Si, Ca/Si, and Ca/Al were used to measure the plagioclase composition. The ratio Na/Ca was not used in order to minimize problems associated with the volatilization of Na under the electron beam.

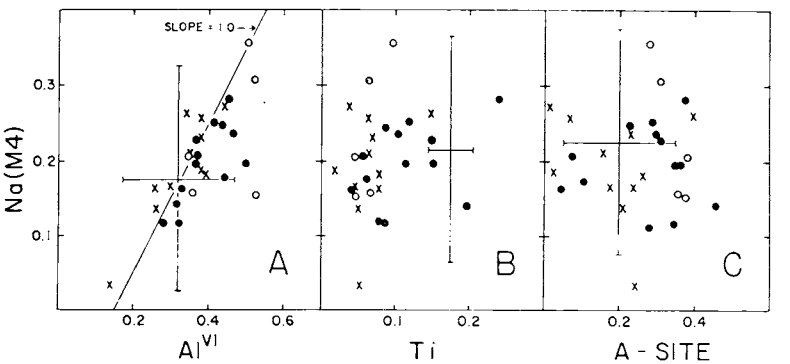

Fig. 9. (A) Plot of Na(M4) versus Al(VI) for amphiboles encountered in this study. (B) Plot of Na(M4) versus Ti for amphiboles encountered in this study. (C) Plot of Na(M4) versus A site occupancy for amphiboles encountered in this study. Symbols as in figure 6.

Measurement of individual ratios on separate feldspar grains from the same experimental charge provided estimates of the feldspar composition that differed sometimes as much as 30 An percent. The large range in An content is attributed to contamination, inasmuch as the association of feldspar grains with small amphibole particles was observed under the petrographic microscope. Plagioclase analyses were corrected using Fe and Mg to monitor the amount of amphibole contamination; the corrected An contents are included in table 3 with the associated amphibole analyses.

There is no systematic change in plagioclase composition within the analytical error over the temperature interval investigated; the measured range in An content is An_{42}-An_{58}. In addition, there is not a significant change in composition between feldspars synthesized on the HM, QFM, and WM buffers. This contrasts with observations from natural amphibolites, which indicate that plagioclase An content increases with metamorphic grade. The lowest temperature feldspars analyzed in this study,

TABLE 5

Electron microprobe analyses of synthetic pyroxenes

	T2-R44 HM Buffer, 883°C, 1.0 kb	T2-102A QFM Buffer, 850°C, 1.0 kb	
	Clinopyroxene	Clinopyroxene	Orthopyroxene
SiO_2	52.32	51.90	51.05
Al_2O_3	2.84	1.41	0.87
FeO	4.86	12.15	28.80
MgO	17.13	14.82	17.05
TiO_2	0.43	0.55	—
MnO	0.37	0.23	0.57
CaO	21.32	18.79	1.44
Na_2O	0.73	0.15	—
Total	100.00*	100.00*	99.78
	Cations per 6 oxygens		
Si	1.900	1.943	1.97
Al^{IV}	0.100	0.057	0.029
Al^{VI}	0.022	0.005	0.011
Fe^{3+}	0.105**	0.031**	0.018**
Fe^{2+}	0.043	0.349	0.911
Mg	0.927	0.827	0.981
Ti	0.012	0.016	—
Mn	0.010	0.007	0.019
Ca	0.830	0.754	0.060
Na	0.051	0.011	—
$\frac{Fe^{2+}}{Fe^{2+} + Mg}$	0.044	0.297	0.482
$\frac{Fe\ tot}{Fe\ tot + Mg}$	0.138	0.315	0.486
$\frac{Fe^{3+}}{Fe^{3+} + Fe^{2+}}$	0.709	0.082	0.018

* Analyses normalized to 100 percent.

** Fe^{3+} calculated from stoichiometry.

however, are from 600°C experiments. Most of the change in plagioclase composition from natural amphibolites occurs between the greenschist and amphibolite facies (400°-525°C). Liou, Kuniyoshi, and Ito (1974) also show the composition of plagioclases from synthesized amphibolites leveling out above 600°C at approximately An_{45}-An_{55}.

RESULTS: PHASE EQUILIBRIA

The phase relations for the olivine tholeiite investigated in this study are characterized by a series of continuous reactions that represent the appearance or disappearance of a phase from the equilibrium assemblage, as displayed in figures 10, 11, 12, and 13. The areas between phase boundaries represent the regions in P–T–f_{O_2} space where a specific assemblage is stable. The phase relations on the WM and QFM buffers (figs. 11 and 12) are topologically similar to each other with only minor differences in the P and T of the reaction boundaries, whereas the phase relations on the HM buffer differ from those on the QFM and WM buffers as follows: (1) ilmenite is replaced by a Ti-rich hematite; (2) at high temperatures (above 735°C) pseudobrookite is present; (3) quartz has been positively identified in over 50 percent of the experiments run on the HM buffer and is suspected to be stable as a minor phase in all experiments; and (4) olivine and orthopyroxene are not stable under any conditions investigated.

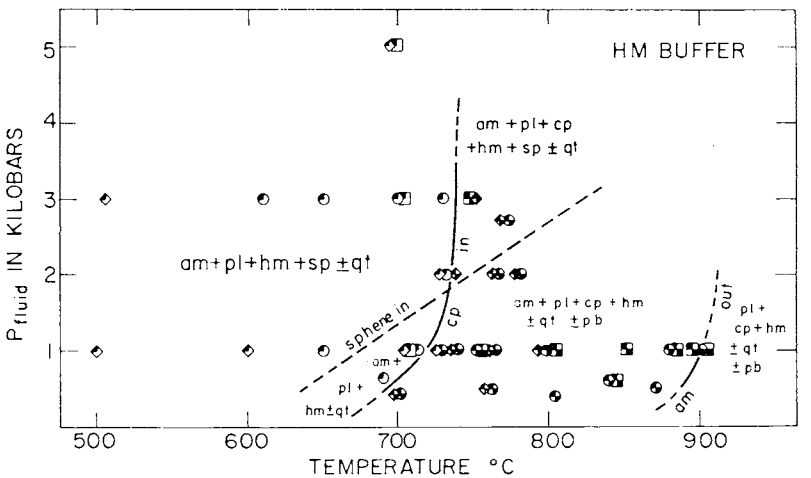

Fig. 10. P_{fluid}-T relations for the basalt V25-RD1-T2 at oxygen fugacities defined by the hematite–magnetite buffer. The starting assemblage is indicated as follows: square = plagioclase + clinopyroxene + olivine + ilmenite or hematite (a basaltic assemblage); circle = plagioclase + clinopyroxene + amphibole + ilmenite or hematite ± orthopyroxene (a granulite facies assemblage); diamond = plagioclase + amphibole + ilmenite or hematite (an amphibole facies assemblage). The phases present in the resulting assemblage are indicated by the part of the symbol that is filled: northwest quadrant = amphibole; northeast quadrant = orthopyroxene; southeast quadrant = clinopyroxene; southwest quadrant = olivine. Abbreviations are as follows: am = amphibole; pl = plagioclase; cp = clinopyroxene; hm = titanohematite; qt = quartz; pb = pseudobrookite; sp = sphene.

The sphene-in reaction.—Below the temperature of the first appearance of clinopyroxene, the assemblages plagioclase + amphibole + ilmenite and plagioclase + amphibole + ilmenite + sphene are stable on the WM and QFM buffers, and plagioclase + amphibole + titanohematite ± quartz and plagioclase + amphibole + titanohematite ± quartz + sphene are stable on the HM buffer. These assemblages exist over a wide range of T-P conditions, and they are separated by the sphene-in reaction curve, with $CaTiSiO_5$ occurring in the lower temperature assemblage.

This reaction was not bracketed by reversal experiments but was determined on the basis of the presence or absence of sphene in the experimental run products. It was possible, however, to produce sphene from both a basaltic and an amphibolitic starting assemblage. In two experiments run at temperatures below the sphene-in reaction boundary (561° and 607°C, 3 kb, QFM buffer) and where the starting material was a previously synthesized amphibolite, sphene was observed rimming the ilmenite. This texture is interpreted as representing a reaction relationship between sphene and ilmenite with decreasing temperature. Sphene was also readily produced by oxidation of the assemblage amphibole + plagioclase + ilmenite on the HM buffer and lost from the assemblage amphibole + plagioclase + titanohematite + sphene + quartz by reduction on the QFM buffer at 750°C, 3 kb. Because of the high reactivity of sphene in this system, it is probable that the postulated sphene-in boundary lies close to the equilibrium boundary.

The upper thermal stability limit of sphene is apparently a strong function of T, P_f, and f_{O_2} as can be seen by comparing the positions of the sphene-in reaction in figures 10, 11, 12 (see also fig. 13). Sphene is favored by low temperature, high pressure, and high oxygen fugacity.

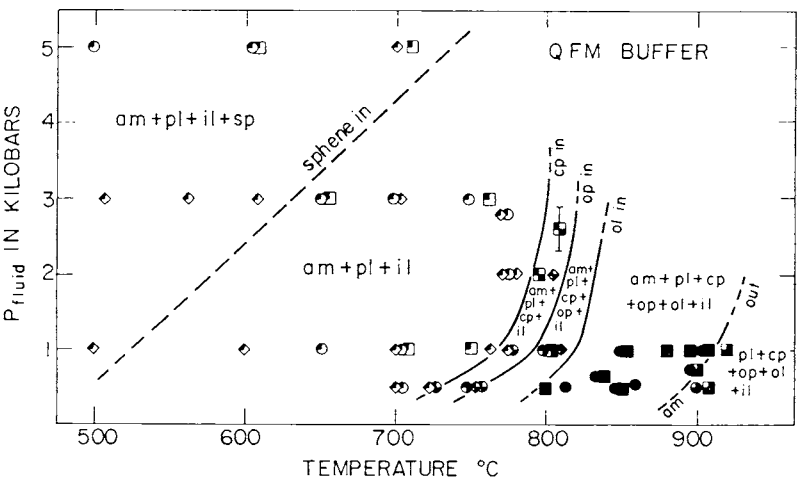

Fig. 11. P_{fluid}-T relations for the basalt V25-RD1-T2 at oxygen fugacities defined by the quartz–fayalite–magnetite buffer. Symbols as in figure 10. Additional symbols include: op = orthopyroxene; ol = olivine; il = ilmenite.

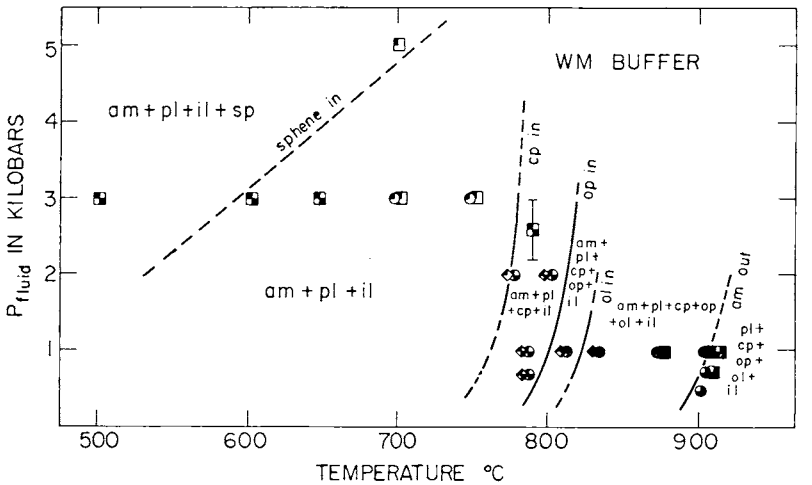

Fig. 12. P_{fluid}-T relations for the basalt V25-RD1-T2 at oxygen fugacities defined by the wüstite–magnetite buffer. Symbols as in figure 10.

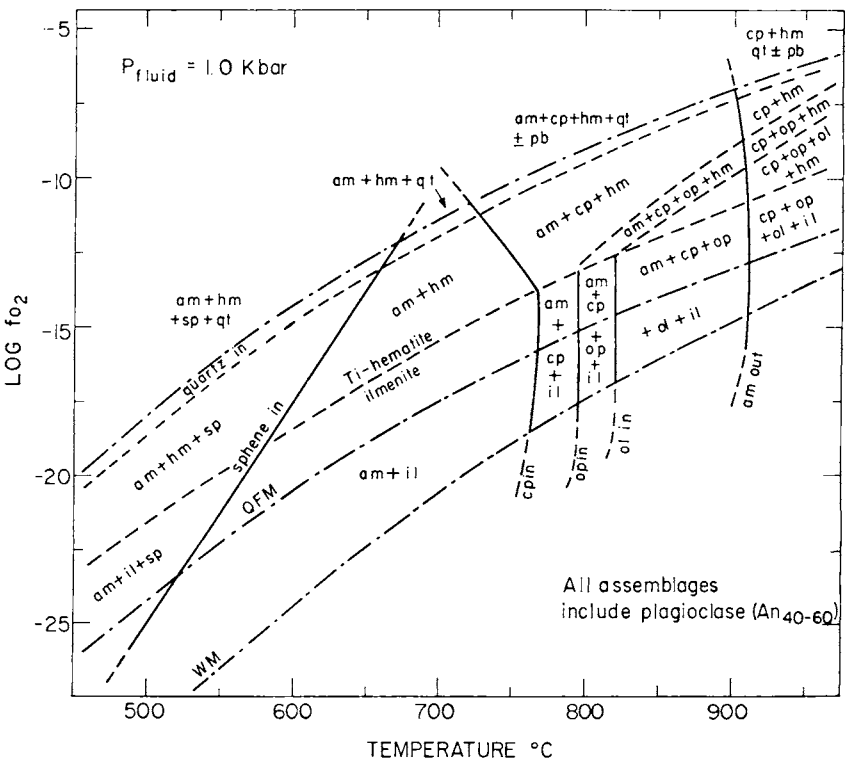

Fig. 13. Phase relations for the basalt V25-RD1-T2 on a log f_{O_2} versus T plot at P_{fluid} = 1 kb. Solid lines are measured phase boundaries, dashed lines are inferred phase boundaries. Dot-dash lines are buffer curves. All assemblages include plagioclase. Abbreviations as in figures 10 and 11.

Evidently the reaction is of the type: oxidized mafic phases + sphene → reduced mafic phases + ilmenite + O_2. It is not known whether the stability of sphene is a function of P_{fluid} or P_{total} inasmuch as the present experiments do not distinguish between these two variables. Deer, Howie, and Zussman (1966) report as much as 0.93 wt percent H_2O+ in analyses of sphene, and it is possible that P_{H_2O} does influence the stability of this phase. Yoder and Tilley (1962, figs. 27, 29, and 30) presented curves for the breakdown of sphene in three different basalts in the melting region. All these curves have very steep negative slopes in contrast to the positive slope obtained by this study for a rock of similar bulk composition. The detailed P-T location of the equilibrium sphene-in boundary in amphibolites must await further work.

The clinopyroxene-in reaction.—With increasing temperature on the HM buffer, amphibole breaks down to clinopyroxene only (+ plagioclase + hematite ± quartz + sphene + H_2O). On the QFM and WM buffers amphibole breaks down to clinopyroxene first and then at successively higher temperatures to clinopyroxene + orthopyroxene and finally clinopyroxene + orthopyroxene + olivine (all reactions include plagioclase + ilmenite + H_2O). The temperature of the clinopyroxene-in, orthopyroxene-in, and olivine-in reactions (table 6) are not tightly bracketed for two reasons: (1) the reactions are difficult to reverse because of the difficulty of nucleating phases (particularly pyroxene) that were not present in the starting material, and (2) it is extremely difficult to detect trace amounts of a phase in these run products.

The heterogeneous reactions involving the incoming of clinopyroxene on the HM, QFM, and WM buffers (as well as the reactions involving the incoming of orthopyroxene and olivine on the QFM and WM buffers) are complex, multivariate reactions. In general, these reactions involve a decrease in the modal abundance of amphibole, as well as a shift in the composition of the amphibole. For the first appearance of clinopyroxene

TABLE 6

Temperature-P_{fluid} coordinates of reaction boundaries

Buffer	P_{fluid} (kb)	Clinopyroxene-in T(°C)	Orthopyroxene-in T(°C)	Olivine-in T(°C)	Amphibole-out T(°C)
HM	0.5	695±10	***	***	—
	1.0	720±9	***	***	902±7
	2.0	735±8	***	***	—
	3.0	738±9	***	***	—
QFM	0.5	730±12	755±10	<800	894±8
	1.0	768±8	794±8	820±15	912
	2.0	788±8	>805	—	—
WM	0.5	—	—	—	895±8
	1.0	<780	798±10	820±12	908±9
	2.0	775±15	—	—	—

*** means phase not present on this buffer.
— means phase present but reaction boundary not determined at these conditions.

at f_{O_2} defined by the QFM and WM buffers, the following reaction can be written:

$$\text{hornblende}_1 + \text{plagioclase}_1 = \text{hornblende}_2 + \text{plagioclase}_2 + \text{clinopyroxene} \pm \text{Fe–Ti oxides} + H_2O. \quad (1)$$

(Hornblende$_2$ is more pargasitic and Ti-rich than hornblende$_1$). A slight increase in modal plagioclase occurs above the clinopyroxene-in reactions (see fig. 14). It is also probable that the anorthite content of the plagioclase increases across the reaction (that is, plagioclase$_2$ is more anorthitic than plagioclase$_1$). The reaction primarily involves the breakdown of the tremolite component in the amphibole to produce clinopyroxene and minor breakdown of the glaucophane component to produce plagioclase; the pargasite and Ti-rich components are concentrated in the residual

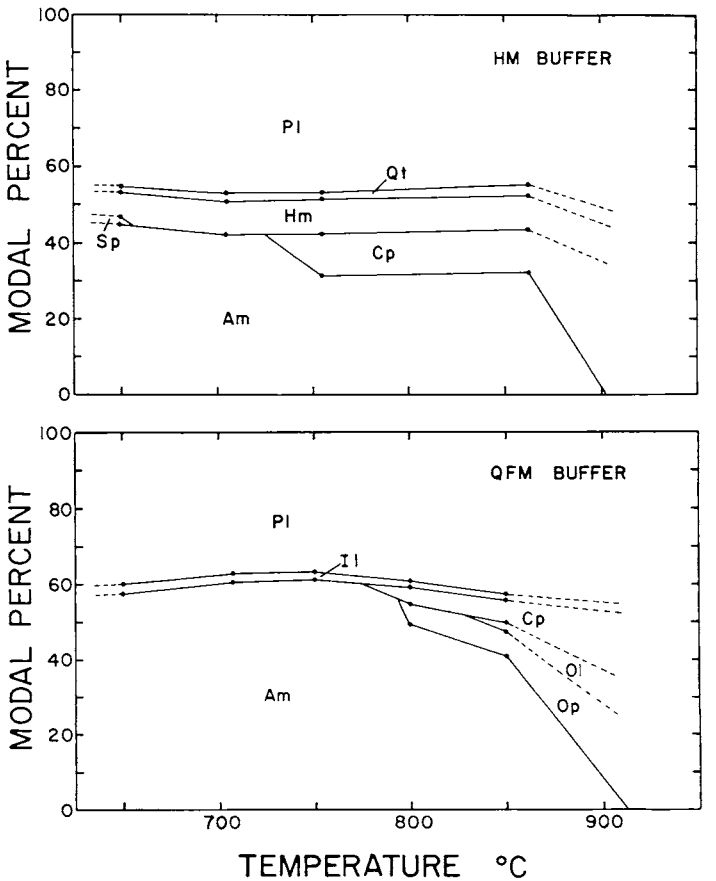

Fig. 14. Calculated modes plotted against temperature at P_{fluid} = 1 kb for experiments run on the HM and QFM buffers. Phases are indicated by the following abbreviations: pl = plagioclase; am = amphibole; il = ilmenite; hm = titanohematite; sp = sphene; qt = quartz; cp = clinopyroxene; op = orthopyroxene; ol = olivine.

hornblende. The reaction for the incoming of clinopyroxene with f_{O_2} defined by the HM buffer is similar to the above reaction except that the compositions of the phases participating in the reaction are different. It is important to note that these are continuous reactions and take place not only at the reaction boundary, but over the entire temperature interval between reaction boundaries.

The orthopyroxene-in reaction.—Orthopyroxene is present only in experiments run on the QFM and WM buffers. Orthopyroxene appears as an equilibrium phase at temperatures between 10° and 30°C above the first appearance of clinopyroxene (table 6). It is clear from the run data in appendix A that the orthopyroxene-in reaction curve has a positive slope on the P_f versus T plot; the curve has been drawn sub-parallel to the clinopyroxene-in reaction curve in figures 11 and 12.

The reaction for the production of orthopyroxene involves a decrease in the modal proportion of hornblende, an increase in the modal proportions of orthopyroxene, clinopyroxene, and plagioclase, and an increase in the Ti and pargasite components of the amphibole. Hence the reaction may be written:

$$\text{hornblende}_2 + \text{plagioclase}_2 = \text{hornblende}_3 + \text{plagioclase}_3 + \text{clinopyroxene} + \text{orthopyroxene} \pm \text{ilmenite} + H_2O. \quad (2)$$

The olivine-in reaction.—Olivine appears as a stable phase approx 20°C above the first appearance of orthopyroxene on the QFM and WM buffers; olivine was not detected in any experiments run on the HM buffer. The following reaction can be written for the production of olivine:

$$\text{hornblende}_3 + \text{plagioclase}_3 = \text{hornblende}_4 + \text{plagioclase}_4 + \text{clinopyroxene} + \text{orthopyroxene} + \text{olivine} \pm \text{ilmenite} + H_2O \quad (3)$$

(where hornblende_4 is even more Ti- and pargasite-rich than hornblende_3).

The amphibole-out reaction.—As shown in figure 13, the upper thermal stability limit of amphibole (that is, the temperature where the concentration of amphibole in the equilibrium assemblage drops to zero) is not markedly influenced by f_{O_2}. However, it is expected that the amphibole-out reaction curves very sharply to low temperature at fluid pressures below 0.5 kb inasmuch as it was very difficult to nucleate amphibole from basalt below this pressure (see figs. 10-12). For reference, the beginning of melting of an olivine tholeiite under conditions of $P_{fluid} = P_{total}$ is approx 20° to 50°C higher than the highest temperature experiments in figures 10, 11, 12, and 13 (from data in Yoder and Tilley, 1962; Helz, 1973; and Holloway and Burnham, 1972). In only a very small region of the diagram at high temperature, low P_{fluid}, and low oxidation state is a basaltic subsolidus assemblage (plagioclase + clinopyroxene + orthopyroxene + olivine + ilmenite) stable. The reaction for the final dehydration of amphibole is:

$$\text{hornblende}_4 = \text{plagioclase} + \text{clinopyroxene} + \text{orthopyroxene} + \text{olivine} + \text{ilmenite} + H_2O \quad (4)$$

on the QFM and WM buffers, and

$$\text{hornblende}_2 = \text{plagioclase} + \text{clinopyroxene} + \text{titanohematite} + H_2O \quad (5)$$

on the HM buffer.

f_{O_2}–T phase relations.—The strong f_{O_2} dependence of the upper thermal stability limit of sphene (see fig. 13) suggests a reaction such as:

$$\text{hornblende}_1 + \text{plagioclase}_1 + \text{sphene} + \text{titanohematite} = \text{hornblende}_2 + \text{plagioclase}_2 + \text{ilmenite} + O_2 + H_2O \quad (6)$$

(where hornblende_2 is more Fe-, Ti-, and pargasite-rich than hornblende_1) for the consumption of sphene.

A reaction boundary corresponding to the hematite–ilmenite solvus (Carmichael, 1961; Lindsley, 1973) has been drawn in figure 13 at oxygen fugacities intermediate between those defined by the QFM and HM buffers. Assemblages stable at oxidation states below this boundary contain ilmenite, whereas above this curve titanohematite is the stable oxide phase. Oxidation of an amphibole + plagioclase + ilmenite-bearing assemblage involves the breakdown of ilmenite to produce titanohematite and the breakdown of Fe-, Ti-, and pargasite-rich components in the amphibole to form plagioclase + titanohematite ± sphene in a reaction similar to reaction (6). Such a reaction is supported by the decrease in modal proportions of amphibole and increase in modal proportions of Fe–Ti oxide and plagioclase with increasing f_{O_2} at constant T and P_f.

The clinopyroxene-in, orthopyroxene-in, olivine-in, and amphibole-out reaction curves have been assigned essentially vertical f_{O_2}–T slopes at oxygen fugacities between those defined by the WM buffer and the ilmenite–hematite solvus. In this region, reactions apparently involve neither comsumption nor liberation of significant amounts of O_2. Below the WM buffer, these reaction boundaries probably curve toward lower temperatures as P_{H_2O} becomes significantly less than P_f by dilution, as f_{H_2} increases in the fluid phase. Above the ilmenite–hematite solvus the clinopyroxene-in and amphibole-out reaction curves trend toward lower temperatures until they intersect the HM buffer curve, above which the phase relations have not been determined.

Orthopyroxene and olivine do not occur in experiments run at f_{O_2} values defined by the HM buffer A topology consistent with observation (but one that has not been verified experimentally) is that the orthopyroxene-in and olivine-in reaction boundaries undergo a strong inflection toward higher temperatures at oxygen fugacities close to those defined by the ilmenite–hematite solvus, as indicated in figure 13. This interpretation is consistent with the data of Helz (1973, fig. 9), in which olivine appears at much higher temperatures in experiments run on the HM buffer than those run on the QFM buffer. Oxidation of the assemblage amphibole + plagioclase + clinopyroxene + orthopyroxene + olivine

+ ilmenite (stable on the QFM buffer at 850°C, P_f = 1 kb) would involve reactions such as:

$$\text{fayalite} + \tfrac{1}{2}\,O_2 = \text{hematite} + \text{quartz} \quad (7)$$

and

$$\text{ferrosilite} + \tfrac{1}{2}\,O_2 = 2\ \text{hematite} + 2\ \text{quartz} \quad (8)$$

These reactions would occur concomitantly with the reaction

$$\text{hornblende}_2 + \text{ilmenite} + O_2 = \text{hornblende}_1 + \text{plagioclase} + \text{titanohematite} + H_2O \quad (9)$$

(where hornblende$_2$ is more Ti-, Fe-, and pargasite-rich than hornblende$_1$). The net result with oxidation (reactions 7 + 8 + 9) is the breakdown of ilmenite, orthopyroxene, olivine, and the Ti-, Fe-, and pargasite-rich components of the amphibole and the production of clinopyroxene, plagioclase, titanohematite, and a more tremolite-rich amphibole. As indicated in figure 14, the oxidation results in an overall reduction in the proportion of amphibole.

The quartz-in reaction boundary has been placed parallel to, and at oxygen fugacities slightly below, the HM buffer curve. At sufficiently high oxidation states, the bulk composition investigated in this study becomes saturated with respect to SiO_2, primarily in response to the oxidation of Fe^{2+} and the production of Fe–Ti oxides. The small amount of quartz present in experiments run on the HM buffer suggests that the quartz-in reaction probably lies close to this buffer curve. It must be emphasized that the presence or absence of quartz in amphibolites is primarily a function of bulk SiO_2 content. Increasing f_{O_2} at constant bulk composition also has the result of increasing the activity of SiO_2.

It is important to note that the upper thermal stability of amphibole is not strongly influenced by the oxygen fugacity. Moreover, within the range of conditions investigated, the temperature of the first appearance of clinopyroxene is only moderately influenced by f_{O_2}. This behavior contrasts sharply with the phase relations of Fe-bearing endmember amphiboles (for example ferropargasite — Gilbert, 1966; ferrotremolite — Ernst, 1966) the upper thermal stability limits of which are very strongly dependent on f_{O_2}. The reason for this difference is clear when the chemical analyses of amphiboles synthesized on the QFM and HM buffers are compared. Amphiboles synthesized on the HM buffer have higher Fe^{3+}/Fe^{2+} and lower Fe^{2+}/Mg than amphiboles synthesized on the QFM buffer. Thus at high f_{O_2}, the amphibole is enriched in components that are either not influenced by f_{O_2} (for example Mg-bearing components) or favored by high oxygen fugacities (for example Fe^{3+}-bearing components).

Calculated modes.—The dehydration of amphibole is a continuous reaction that involves the change in chemical composition and modal proportion of phases over the reaction interval. In order to monitor these changes, an estimate of the modal amounts of phases present in the synthetic run products was obtained by means of a least squares calcula-

tion based on the measured mineral compositions. Results for experiments employing the HM and QFM buffers at P_f = 1 kb are plotted against temperature in figure 14. The calculated modes agree to within approx 10 relative percent of modes estimated from petrographic observation.

Figure 14 graphically displays the sympathetic increase in amphibole breakdown products with the decrease in amphibole proportions. Also apparent is the difference in modal proportions of amphibole between experiments equilibrated on the QFM and HM buffers. It is of interest to note that for both f_{O_2} ranges, amphibole does not begin to decrease sharply in modal amount until within approx 25° to 50°C of its ultimate breakdown temperature. Thus the relative proportion of amphibole + breakdown products does not provide a very sensitive indication of temperature.

GEOLOGIC APPLICATIONS

The Amphibolite Facies

The results of this study demonstrate that for a rock of olivine tholeiite composition, a "typical" amphibolite assemblage consisting predominantly of hornblende + plagioclase exists over a wide range of temperatures, pressures, and oxygen fugacities with $P_{H_2O} = P_{total}$. The upper limit of this association is marked by the beginning of the breakdown of amphibole to form clinopyroxene. The lower limit of hornblende + plagioclase was not determined in this study, but Liou, Kuniyoshi, and Ito (1974) found that chlorite begins to grow from the assemblage hornblende + plagioclase + quartz at temperatures below 550°C, P_{H_2O} = 2 kb, QFM buffer. Below 475°C the hornblende + plagioclase + quartz assemblage is entirely replaced by the greenschist facies assemblage actinolite + chlorite + epidote + albite + quartz. Hence the amphibolite facies assemblage hornblende + plagioclase is stable over 175° to 200°C where $P_{H_2O} = P_{total} = 3 \pm 2$ kb. This temperature range places rather broad limits on temperature estimates for the amphibolite facies; however, hornblende and plagioclase react continuously over this temperature range, which results in changes in the composition of these phases and allows an estimate of the conditions of metamorphism.

Two reaction boundaries that mark the appearance or disappearance of a phase have been detected over this temperature range, and these might prove useful in estimating conditions of metamorphism. One, marking the first appearance of sphene, is a strong function of f_{O_2} and P_{H_2O}, although it is not known at this time what the effect of $P_{H_2O} < P_{total}$ is on this boundary. The presence of sphene is favored by low T, high P_{H_2O}, and high f_{O_2}, although bulk composition is also critical in determining the stability of sphene (Helz, 1973). Laird (ms) observed that sphene is the common Ti-bearing phase in low grade amphibolites, whereas ilmenite, rutile, or hematite is the common phase in higher grade assemblages. Thus sphene may serve as a useful mineral with which to

subdivide the amphibolite facies. The second reaction boundary separates the regions where quartz is present from the region where quartz is absent from the assemblage. For the bulk composition studied here, the presence of quartz was entirely determined by the f_{O_2} of the experiment, although bulk SiO_2 content undoubtedly plays a major role in influencing the stability of quartz.

The Granulite Facies

In the progressive metamorphism of amphibolite, clinopyroxene typically appears at lower metamorphic grade than orthopyroxene (Engel and Engel, 1962a; Stoddard, ms). The first appearance of orthopyroxene generally is taken as the index mineral for the onset of granulite facies P-T conditions (Winkler, 1974; Turner, 1968). The present study has shown: (1) at constant P_f, orthopyroxene first appears between 10° to 30°C higher than the first appearance of clinopyroxene at low f_{O_2}; (2) the temperature of the first appearance of orthopyroxene is a function of P_f; and (3) at sufficiently high f_{O_2}, orthopyroxene is not stable at all.

Under conditions of $P_{fluid} = P_{total}$, the first appearance of orthopyroxene occurs at temperatures of 780° to 800°C, 1 kb and greater than 805°C, 2 kb on the QFM buffer. Binns (1968) investigated the breakdown of hornblende$_1$ + quartz = hornblende$_2$ + orthopyroxene + Ca–clinopyroxene + plagioclase + H_2O. He reported temperatures for the incoming of orthopyroxene for experiments run on the QFM buffer of 760°C, 1 kb and 780°C, 2 kb. In the system studied by Binns (1968), clinopyroxene and orthopyroxene apparently appeared at the same temperature.

Choudhuri and Winkler (1967) investigated the reaction defining the lower limit of the pyroxene hornfels facies, hornblende$_1$ + anthophyllite = hornblende$_2$ + enstatite + anorthite + H_2O. Hornblende in the presence of anthophyllite begins to dehydrate to enstatite and anorthite at 715°C, 1 kb, and final dehydration to enstatite + diopside + anorthite takes place at 770°C, 1 kb. Hornblende coexists with orthopyroxene and anorthite over this temperature range; there is no indication that hornblende decreases in amount over this range of temperature or changes composition over the reaction interval according to Choudhuri and Winkler.

The effect of SiO_2 saturation on the first appearance of orthopyroxene.—Amphiboles saturated with respect to SiO_2 (for example tremolite; Boyd, 1959) have a lower upper thermal stability limit than amphiboles undersaturated with respect to SiO_2 (for example pargasite; Boyd, 1959). The system studied by Binns (1968) was SiO_2 saturated, and orthopyroxene appeared 35°C lower than in the present study. Other bulk composition differences may in part account for this difference, but it is suspected that SiO_2 saturation is the dominant influence.

Eight experiments were run with excess quartz added to the rock used in the present study. The experiments do not bracket the orthopyroxene-in reaction, but orthopyroxene did grow at temperatures as low as 745°C, 1 kb, QFM buffer. The results of these experiments strongly

suggest that SiO_2 saturation may decrease the temperature of the first appearance of orthopyroxene by as much as 50°C.

The effect of Fe/Mg on the production of pyroxene.—The effect of Fe/Mg on the first appearance of pyroxene can be qualitatively evaluated by analogy with other Fe:Mg solid solutions. Wones and Eugster (1965) determined the upper thermal stability limit of a biotite with a specified Fe/Mg as a function of P_{fluid} and f_{O_2}. For a binary amphibole join such as tremolite–ferrotremolite or pargasite–ferropargasite, f_{O_2} versus T relationships should be topologically similar to those of biotite. At a given oxygen fugacity buffer, then, an increase in bulk Fe/Mg should result in a decrease in the temperature of the first appearance of pyroxene in a binary Fe:Mg amphibole system such as pargasite–ferropargasite.

In an amphibolite consisting of hornblende + plagioclase + Fe–Ti oxides, the effect of changing bulk rock Fe/Mg on the temperature of the first appearance of orthopyroxene should not be as pronounced as in a binary Fe:Mg amphibole system. The difference is due to the fact that in a complex amphibolite, the amphibole composition can change away from a binary Fe:Mg solid solution through reactions such as (6) and (9) and thus remain stable to higher temperatures than would be possible were it constrained to a binary Fe:Mg solid solution.

Calculation of amphibole breakdown with $P_{H_2O} < P_{total}$.—Data from this and other studies indicate that temperatures for the first appearance of orthopyroxene in rocks of amphibolitic composition range from approx 740° to 800°C depending on the bulk composition, at $P_{H_2O} = 1$ to 2 kb. Totally anhydrous (amphibole-free) subsolidus assemblages can only exist at temperatures in excess of 900°C and with P_{H_2O} less than approx 1 kb; at higher fluid pressures partial melting is encountered. Independently derived temperature estimates for granulite facies metamorphism are typically much lower than these values. For example, Stoddard (ms) estimated a temperature of 730° ± 30°C for metamorphism in the Colton-Rainbow Falls, northwest Adirondack Mountains, New York. The complete dehydration of amphibole at temperatures less than those reported here requires values of P_{H_2O} less than P_{total}.

To evaluate the effect of $P_{H_2O} < P_{total}$, consider the assemblage stable above the clinopyroxene-in reaction: hornblende + clinopyroxene + quartz + plagioclase + Fe–Ti oxides (T = 750°C, P_{H_2O} = 2 kb, HM buffer). The following stoichiometric relationship can be written among components of the phases in this assemblage:

$$Ca_2Mg_5Si_8O_{22}(OH)_2 = 2CaMgSi_2O_6 + 3\ MgSiO_3 + SiO_2 + H_2O.$$

This expression can be written in terms of chemical potentials and rearranged to yield

$$\Delta\mu^\circ + RT \ln \frac{a_{Di}^2 a_{En}^3}{a_{Tr}} + RT \ln f_{H_2O} = 0,$$

in which a_{Di} is the activity of the diopside component in clinopyroxene,

a_{En} is the activity of the enstatite component in clinopyroxene, and a_{Tr} is the activity of the tremolite component in hornblende. A least-squares regression by Ferry (ms) of the data presented by Boyd (1959) for the breakdown of tremolite yields the expression $\Delta\mu^\circ = 29442 - 39.501T - 0.572P$. Using this relation for $\Delta\mu^\circ$ and data for f_{H_2O} from Burnham, Holloway, and Davis (1969), the above equation can be solved for the equilibrium constant, $K_{eq} = (a_{Di}^2 a_{En}^3/a_{Tr})$, at any T and P. At conditions just above the first appearance of clinopyroxene on the HM buffer (750°C, P = 2 kb), the value of $K_{eq} = 0.264$.

This is the value of K_{eq} under conditions of $P_{H_2O} = P_{total}$. Under conditions where $P_{H_2O} < P_{total}$, amphibole will begin to break down to clinopyroxene at lower T. Using the above value for the equilibrium constant and the relation provided by Ferry (ms), it is possible to calculate the f_{H_2O} for the first appearance of clinopyroxene at any T. At 700°C, $P_{total} = 2$ kb, the calculation yields a value of $f_{H_2O} = 717$ bars. If species in the metamorphic fluid mix ideally, the Lewis and Randall rule (Lewis and Randall, 1961) can be applied to calculate the mole fraction of H_2O in the fluid. For the above conditions, the calculation yields a value of $X_{H_2O} = 0.53$. Therefore, if H_2O were diluted to approximately half the concentration of a pure H_2O fluid, clinopyroxene would be stable at a temperature of 700°C, $P_{fluid} = 2$ kb, HM buffer. Changing the value of K_{eq} by ± 20 percent results in calculated values of f_{H_2O} of 597 bars and 897 bars ($X_{H_2O} = 0.44$ and 0.67, respectively), hence the calculation must be considered only as an approximation. Total pressure does not affect the calculations greatly: the same calculation for $P_{total} = 8$ kb yields $X_{H_2O} = 0.49$.

Using data from Binns (1968) for the dehydration of hornblende to orthopyroxene + clinopyroxene (T = 780°C, $P_{H_2O} = 2$ kb, QFM buffer), the calculation yields a value of f_{H_2O} of 503 bars, or $X_{H_2O} = 0.38$ for the first appearance of orthopyroxene at 700°C.

The complete dehydration of hornblende occurs at approx 910°C, $P_{H_2O} = P_{total} = 2$ kb, HM buffer (extrapolated from data in this study). For these conditions, the calculation yields a value of $f_{H_2O} = 131$ bars, or $X_{H_2O} = 0.1$ for the complete dehydration of amphibole at 700°C with $P_{H_2O} < P_{total}$.

The purpose of these calculations is to estimate the magnitude of dilution of H_2O in the fluid phase necessary to promote the dehydration of amphiboles at T = 700°C. Although the calculations must be considered approximate, the values of f_{H_2O} and X_{H_2O} derived are reasonable for the partial and complete dehydration of amphibole at temperatures of the granulite facies. Essene, Bohlen, and Valley (1978) have calculated water fugacities of 316 to 1995 bars for metamorphism in the Adirondacks. Fluid inclusion studies (Touret, 1971; Hollister and Burruss, 1976) indicate that the fluid present in granulite facies metamorphism is

composed largely of CO_2, whereas in the amphibolite facies, the fluid is dominately H_2O. This change in the H_2O to CO_2 ratio in the metamorphic fluid between the amphibolite and the granulite facies is a likely mechanism for producing the dehydration of amphibole at temperatures of 650° to 700° C and conditions of $P_{fluid} = P_{total}$.

ACKNOWLEDGMENTS

This study was carried out during the tenure of a National Defense Educational Act Title IV fellowship, teaching and research assistantships at the University of California, Los Angeles, and a predoctoral fellowship at the Geophysical Laboratory, Carnegie Institute of Washington.

Experimental work was supported by National Science Foundation grant EAR 77-10649/Ernst and Penrose grant 2018-75. Electron microprobe analyses were performed at the University of California, Los Angeles with support of N.S.F. grant DES 74-22672 (Ernst) and a grant from the University of California Patent Fund.

I wish to acknowledge gratefully the continual support, guidance, and encouragement of W. G. Ernst who served as my advisor during this study.

The manuscript in some form has been critically read and improved by W. A. Dollase, W. G. Ernst, J. M. Ferry, R. T. Helz, J. R. Holloway, D. D. Jackson, C. M. Knobler, T. C. Labotka, J. J. Papike, D. Rumble, III, H. S. Yoder, N.B.N.M.S.

I also wish to acknowledge helpful discussions with W. W. Wegner, E. F. Stoddard, W. P. Freeborn, and J. L. Rosenfeld.

APPENDIX A
Results of hydrothermal experiments

Run #	Starting Assemblage	T°C	P_{fluid} bars	Duration (hours)	Resulting Assemblage
			HM BUFFER		
T2-R46	pl+cp+am(tr)+hm	871	500	254	pl+cp(dec)+am(inc)+hm
T2-R42A	pl+cp+hm	842	600	477	pl+cp+am(inc)+hm+qt
T2-R45A	pl+cp+am(tr)+il	842	600	477	pl+cp+am(inc)+hm+qt
T2-R7	pl+cp+am+hm	804	400	244	pl+cp+(inc)+am(dec)+hm(inc)+qt(?)+pb
T2-R60A	pl+am+il	759	500	447	pl+cp(tr)+am+hm+pb
T2-R53A	pl+cp+am+il	759	500	447	pl+cp(tr)+am+hm+pb
T2-R52A	pl+cp+am+il	700	450±50	981	pl+cp(tr)+am+hm
T2-R59A	pl+am+il	700	450±50	981	pl+cp(tr)+am+hm
T2-R114	pl+cp(tr)+am+hm+qt	690	650	735	pl+am+hm+qt
T2-R69A	pl+cp+ol+il	901	1000	247	pl+cp+hm
T2-R70A	pl+cp+am+hm	901	1000	247	pl+cp+am(dec)+hm+qt
T2-122	pl+cp+ol+il	897	1000	42	pl+cp+am(tr)+hm
T2-R40	pl+cp+hm	883	1000	169	pl+cp+am(tr)+hm+qt
T2-R44	pl+cp+am(tr)+hm	883	1000	169	pl+cp(dec)+am(inc)+hm
T2-121	pl+cp+ol+il	852	1000	92	pl+cp+am+hm
T2-123	pl+cp+ol+il	804	1000	93	pl+cp(dec)+am+hm
T2-R89	pl+cp+am+il	799	1000	195	pl+cp+am+hm+pb
T2-R88	pl+am+il	799	1000	195	pl+cp+am+hm+pb
T2-R51	pl+cp+ol+il	762	1000	233	pl+cp(tr)+am+hm+pb+qt(?)
T2-R58	pl+am+il	762	1000	233	pl+cp+(tr)+am+hm+pb+qt(?)
T2-45B	pl+cp+ol+il	754	1000	695	pl+cp+am+hm+qt
T2-R98	pl+cp(tr)+am+il	736	1000	339	pl+cp(inc)+am+hm+pb
T2-R800	pl+cp+am+il	736	1000	177	pl+cp+am+hm+pb+qt
T2-R790	pl+am+hm	736	1000	177	pl+cp(tr)+am+hm+pb
T2-R111	pl+am+hm	728	1000	279	pl+am+hm
T2-R113	pl+cp+am+hm	728	1000	279	pl+cp(tr)+am+hm
T2-R50	pl+cp(tr)+am+il	713	1000	430	pl+am+hm+qt
T2-R57A	pl+am+il	706	1000	574	pl+am+hm+qt
T2-124A	pl+cp+ol+il	706	1000	574	pl+am+hm+qt
T2-R106	pl+cp+am+il	650	1000	357	pl+am+hm+sp+qt
T2-R102	pl+am+il	600	1000	2723	pl+am+hm+qt+sp
T2-R18A	pl+am+il	503	1000	2494	pl+am+hm+qt+sp
T2-R820	pl+cp+am+il	779	2000	204	pl+cp+am+hm+qt
T2-R810	pl+am+il	779	2000	204	pl+cp+am+hm+qt
T2-R47A	pl+cp(tr)+am+il	765±6	2000	437	pl+cp+am+hm+qt
T2-R54A	pl+am+hm	765±6	2000	437	pl+cp(tr)+am+hm+qt
T2-R110	pl+am+hm	738	2000	279	pl+cp(tr)+am+hm+sp
T2-R48	pl+cp(tr)+am+il	729	2000	361	pl+am+hm+sp+qt
T2-R55	pl+am+il	729	2000	361	pl+am+hm+sp+qt
T2-R49	pl+cp(tr)+am+il	771	2700±100	194	pl+cp(tr)+am+hm+sp
T2-R56	pl+am+il	771	2700±100	194	pl+cp(tr)+am+hm+sp
T2-40B	pl+cp+ol+il	748	3000	637	pl+cp(tr)+am+hm+qt?+sp
T2-162B	pl+am+hm+sp	752	3000	887	pl+cp(tr)+am+hm+sp
T2-R115	pl+cp+am+hm+qt+sp	730	3000	279	pl+am+hm+qt?+sp
T2-125A	pl+cp+ol+il	701	3000	628	pl+am+hm+qt+sp
T2-R97	pl+cp+am+il	701	3000	237	pl+am+hm+qt+sp
T2-R107	pl+cp+am+il	651	3000	300	pl+am+hm+sp
T2-R103	pl+cp+am+il	610	3000	427	pl+am+hm+sp
T2-R87	pl+am+il	505	3000	519	pl+am+hm+qt+sp
T2-126A+	pl+cp+ol+il	698	5000	534	pl+am+hm+qt+sp
T2-R96	pl+am+il	695	5000	190	pl+am+hm+qt+sp

APPENDIX A (continued)

Run #	Starting Assemblage	T°C	P_{fluid} bars	Duration (Hours)	Resulting Assemblage
			QFM BUFFER		
T2-109	pl+cp+ol+il	908	500	194	pl+cp+ol+il+op
T2-R750	pl+cp+am+ol+il	899	500	87	pl+cp+ol+il+op
T2-R740	pl+cp+ol+il	897	750	153	pl+cp+ol+il+op
T2-R730	pl+cp+am+ol+il	897	750	153	pl+cp+am(tr)+ol+il+op
T2-R5	pl+cp+am+il	859	520	128	pl+cp(inc)+am(dec)+ol+il+op
T2-R23	pl+cp+ol+il	850	380	142	pl+cp+am+ol+il+op
T2-R21	pl+cp+am+ol+il	850	380	142	pl+cp(inc)+am(dec)+ol+il+op?
T2-R24	pl+cp+ol+il	835	650	196	pl+cp+am(tr)+ol+il+op
T2-R22	pl+cp+am+ol+il	835	650	196	pl+cp(dec)+am(inc)+ol+il+op
T2-R6	pl+cp+am+il	814	517	128	pl+cp(inc)+am(dec)+il+ol+op
T2-110	pl+cp+ol+il	800	500	138	pl+cp+am?+ol+il+op
T2-R31	pl+cp+am+ol+il	754	500	408	pl+cp(dec)+am+il
T2-R38	pl+am+il	754	500	408	pl+cp(tr)+am+il
T2-118	pl+cp+am+il	750	500	198	pl+cp+am+il+op(tr)
T2-R710	pl+am+il	725	500	384	pl+am+il
T2-R720	pl+cp+am+il	725	500	384	pl+cp(tr)+am+il
T2-R29A	pl+cp+am+il	702	500	768	pl+am+il
T2-R36A	pl+am+il	702	500	768	pl+am+il
T2-106	pl+cp+ol+il	920	1000	193	pl+cp+ol+il+op
T2-R780	pl+cp+ol+il	904	1000	137	pl+cp+am(tr)+ol+il+op
T2-R770	pl+cp+am+ol	904	1000	137	pl+cp+am+ol+il+op
T2-107	pl+cp+ol+il	896	1000	195	pl+cp+am(tr)+ol+il+op
T2-96	pl+cp+ol+il	880	1000	26	pl+cp+am(tr)+ol+il+op
T2-102A	pl+cp+ol+il	850	1000	291	pl+cp+am+ol(tr)+il+op
T2-R90	pl+cp+am+il	850	1000	291	pl+cp+am+ol(tr)+il+op
T2-R33	pl+am+il	804	1000	213	pl+cp+am+il+op
T2-R26A	pl+cp+am+il	802	1000	408	pl+cp+am+il+op
T2-116A	pl+cp+ol+il	802	1000	288	pl+cp+am+il+op
T2-R25A	pl+cp+am+il	775	1000	510	pl+cp(tr)+am+il
T2-R32A	pl+am+il	775	1000	510	pl+am+ilm
T2-R117	pl+am+il	762	1000	264	pl+am+il
T2-58A	pl+cp+ol+il	750	1000	1770	pl+am+il
T2-81A	pl+cp+ol+il	707	1000	574	pl+am+il
T2-R108	pl+am+il	703	1000	165	pl+am+il
T2-R93	pl+cp+am+il	703	1000	165	pl+am+il
T2-R104	pl+cp+am+il	651	1000	357	pl+am+il
T2-R101	pl+am+il	559±8	1000	437	pl+am+il
T2-R17A	pl+am+il	499	1000	2497	pl+am+il+sp
T2-R35	pl+am+il	804	1995	214	pl+cp(tr)+am+il
T2-50A	pl+cp+ol+il	795	2000	405	pl+cp(tr)+am+il
T2-R116	pl+am+il	779	2000	264	pl+am+il
T2-R27	pl+cp+am+il	773	2000	295	pl+am+il
T2-R34	pl+am+il	773	2000	295	pl+am+il
T2-115	pl+cp+ol+il	809	2600±300	102	pl+cp(tr)+am+il
T2-R30	pl+cp+am+il	771	2800	214	pl+am+il
T2-R37	pl+am+il	771	2800	214	pl+am+il
T2-54A	pl+cp+ol+il	763	3000	1243	pl+am+il
T2-161B	pl+cp+am+hm+qt+sp	749	3000	887	pl+am+il
T2-61A	pl+cp+ol+il	699	3000	1060	pl+am+il
T2-R95	pl+cp+am+il	699	3000	336	pl+am+il
T2-55A	pl+cp+ol+il	655	3000	1160	pl+am+il
T2-R105	pl+cp+am+il	650	3000	300	pl+am+il

APPENDIX A (continued)

Run #	Starting Assemblage	T°C	P_{fluid} bars	Duration (Hours)	Resulting Assemblage
T2-85A	pl+am+il	607	3000	761	pl+am+il+sp
T2-86	pl+am+il	561	3000	334	pl+am+il+sp
T2-87A	pl+am+il	506	3000	853	pl+am+il+sp
T2-77A	pl+cp+ol+il	710±8	5000	471	pl+am+il+sp
T2-R11A	pl+am+il	700	5000	477	pl+am+il+sp
T2-78A	pl+cp+ol+il	606	5000	777	pl+am+il+sp
T2-R12A	pl+cp+ol+il	606	5000	1872	pl+am+il+sp
T2-R10A	pl+cp+am+il	498	5000	2088	pl+am+il+sp
			WM BUFFER		
T2-R61	pl+cp+am+ol+il	901	500	145	pl+cp+ol(inc)+il+op
T2-R62	pl+cp+am+ol+il	906	750	143	pl+cp+ol(inc)+il+op
T2-R66	pl+cp+ol+il	906	750	143	pl+cp+ol+il+op
T2-R81	pl+am+il	785	700	141	pl+cp(inc)+am+il
T2-R74	pl+cp(tr)+am+il	785	700	141	pl+cp(inc)+am+il
T2-129	pl+cp+ol+il	909	1000	96	pl+cp+ol+il+op
T2-R63A	pl+cp+am+ol+il	907	1000	262	pl+cp+am(tr)+ol+il+op
T2-R67A	pl+cp+ol+il	907	1000	262	pl+cp+am(tr)+ol+il+op
T2-R64	pl+cp+am+ol+il	875	975	120	pl+cp(dec)+am(inc)+ol+il+op
T2-R68	pl+cp+ol+il	875	975	120	pl+cp(dec)+am(inc)+ol+il+op
T2-R78A	pl+am+il	831	1000	223	pl+cp+am+ol+il+op
T2-R71A	pl+cp+am+il	831	1000	223	pl+cp+am+ol(tr)+il+op
T2-R83A	pl+am+il	809	1000	207	pl+cp+am+il+op
T2-R76A	pl+cp+am+il	809	1000	207	pl+cp+am+il+op
T2-R80	pl+am+il	784	1000	141	pl+cp(tr)+am+il
T2-R73	pl+cp+am+il	784	1000	141	pl+cp(tr)+am+il
T2-R79	pl+am+il	798	2000	85	pl+cp(tr)+am+il
T2-R72	pl+cp+am+il	798	2000	85	pl+cp(tr)+am+il
T2-R84	pl+am+il	774	2000	153	pl+am+il
T2-R77	pl+cp+am+il	774	2000	153	pl+cp(tr)+am+il
T2-131	pl+cp+ol+il	790	2600±400	141	pl+cp(tr)+am+il
T2-73B	pl+cp+ol+il	750	3000	649	pl+am+il
T2-R100	pl+cp+am+il	748	3000	189	pl+am+il
T2-130A	pl+cp+ol+il	700	3000	537	pl+am+il
T2-R99	pl+cp+am+il	697	3000	237	pl+am+il
T2-72B	pl+cp+ol+il	647	3000	661	pl+cp(tr-r)+am+il
T2-71A	pl+cp+ol+il	603	3000	826	pl+cp(dec-r)+am+il+sm
T2-84	pl+cp+ol+il	501	3000	413	pl+cp(dec-r)+am(tr)+il+sm+sp
T2-132B	pl+cp+ol+il	700	5000	664	pl+am+il+sp

Abbreviations used in the table include: pl = plagioclase; cp = clinopyroxene; op = orthopyroxene; ol = olivine; am = amphibole; sp = sphene; il = ilmenite; hm = titanohematite; pb = pseudobrookite; sm = smectite; and qt = quartz. Other abbreviations include: tr = the phase is present in trace amounts (less than 2%); inc = the phase is increasing in modal amount; dec = the phase is decreasing in modal amount; and r = the phase is interpreted as being relict.

APPENDIX B

Description and significance of smectite produced in hydrothermal experiments

An expandable lattice clay mineral occurs in all runs below 650°C in which the starting material is a crystalline basalt. The phase forms rapidly, being produced in runs of only a few hrs duration, and persists for over 2000 hrs in runs below 550°C. The phase does not occur in runs where the starting material is an amphibolite assemblage.

The expandable lattice clay mineral is given the generic name smectite, which includes all expandable lattice clays. Individual crystals of smectite are not resolved under the petrographic microscope, but clusters of smectite can be observed. The mineral is green with an average refractive index of approx 1.58. The (001) basal reflection of the synthetic smectite is typically 14A and can easily be collapsed to 9.6A by heating or expanded to 17A by treatment with ethylene glycol. Under the scanning electron microscope, smectite appears as platelets up to 5μm in diameter with a diameter to thickness ratio of 10:1 to 20:1. It could not be resolved whether the platelets were single crystals or aggregates, although no grain boundaries could be resolved within the platelets.

The stability of smectite in these experiments could not be unequivocally determined. The phase is probably metastable in all runs above approx 450°C for the following reasons: (1) smectite occurs in assemblages containing relict (metastable) pyroxenes; (2) smectite is produced only in experiments made directly from a crystalline basalt and not in runs where the starting assemblage is amphibole + plagioclase; (3) in experiments of over 1000 hrs duration the amount of smectite decreases in rough proportion to the decrease in the amount of pyroxene; (4) in one experiment (500°C, 1 kb, 1786 hrs, no buffer), a 14A chlorite was produced at the expense of smectite; and (5) smectites are not found in regionally metamorphosed rocks of similar composition to that studied here, the stable phase being chlorite.

Semiquantitative analyses of smectites synthesized on the HM and QFM buffers were obtained using an energy dispersive (SiLi) detector (table 7). The samples were prepared by allowing the clay minerals to settle in water onto a polished diamond. An accelerating potential of 15kV and sample current of 5nA were used to minimize sample damage. Integrated peak areas for the unknown were compared to an amphibole

TABLE 7

Electron microprobe analyses of smectite

	T2-42A*		T2-63A**	
SiO_2	45.12		45.48	
Al_2O_3	11.98		12.23	
TiO_2	0.45		0.0	
FeO***	5.09		15.69	
MgO	32.37		22.25	
CaO	0.00		1.10	
Na_2O	4.13		2.44	
K_2O	0.87		0.82	
	100.0		100.0	
Si	5.868	7.731	6.141	8.088
Al	1.836		1.947	
Fe^{2+}	0.553	6.872	1.772	6.249
Mg	6.275		4.477	
Ti	0.044		0.0	
Ca	0.0		0.159	
Na	1.040	1.185	0.639	0.939
K	0.145		0.141	
Fe/Mg	0.09		0.40	

* T2-42A run conditions are: 550°C, 3 kb, HM buffer, 1315 hours total.
** T2-63A run conditions are: 506°C, 3 kb, QFM buffer, 2032 hours total.
*** All Fe computed as FeO.

standard spectrum, and the results normalized to 100 percent. Replicate analyses indicate that the precision is approx ± 10 percent of the amount present for major elements.

Comparison with wet chemical analyses from Deer, Howie, and Zussman (1962, v. 3, table 39) reveals that the synthetic smectite produced in this study most closely resembles saponite in composition, the ideal formula for which is $Si_{7.34}Al_{0.66}Mg_{6.0}(1/2Ca,Na)_{0.66}$. The smectites from the present study have considerably more iron than ideal saponites, but one analysis from Deer, Howie, and Zussman (1962, v. 3, table 39, analysis 15) compares favorably with the high iron saponite in sample T2-63A.

Chemical analyses of saponites from altered oceanic basalt have been reported by Melson and Thompson (1973) and Banks (1972). The saponites reported here are similar to those reported by Banks but contain considerably more Na and less K than those analyzed by Melson and Thompson.

The most striking feature of the analyzed smectites in table 7 is the difference in chemistry between the saponites produced in the HM and QFM buffers — particularly in Fe/Mg. A shift toward lower Fe/Mg, especially where the Fe is Fe^{2+}, is typical in silicates at high oxygen fugacities (see data on amphibole chemistry). It is conceivable, therefore, that saponite may be used as an indicator of f_{O_2} of formation in rocks where it occurs. This would be particularly revealing for saponite from metamorphosed oceanic basalts, inasmuch as the conditions of metamorphism of these rocks are not at all well understood.

References

Armstrong, J. T., and Buseck, P. R., 1975, Quantitative chemical analysis of individual microparticles using the electron microprobe: theoretical: Anal. Chemistry, v. 47, p. 2178-2192.

Banks, H. Jr., 1972, Iron-rich saponite: additional data on samples dredged from the mid-Atlantic Ridge, 22°N: Smithsonian Contr. Earth Sci., no. 9, p. 39-42.

Binns, R. A., 1965a, Hornblendes from some basic hornfelses in the New England region, New South Wales: Mineralog. Mag., v. 34, p. 52-65.

———— 1965b, The mineralogy of metamorphosed basic rocks from the Willyama Complex, Broken Hill district, New South Wales, Pt. I. Hornblendes: Mineralog. Mag., v. 35, p. 305-326.

———— 1968, Hydrothermal investigations of the amphibolite–granulite facies boundary: Geol. Soc. Australia Spec. Pub. 2, p. 341-344.

Boyd, F. R., 1959, Hydrothermal investigations of amphiboles, *in* Abelson, P. H., ed., Researches in Geochemistry: New York, John Wiley & Sons, Inc., p. 377-396.

Brown, E. H., 1977, The crossite content of Ca-amphibole as a guide to pressure of metamorphism: Jour. Petrology, v. 18, p. 53-72.

Burnham, C. W., Holloway, J. R., and Davis, N. F., 1969, Thermodynamic properties of water to 1000°C and 10,000 bars: Geol. Soc. America Spec. Paper 132, 96 p.

Carmichael, C. M., 1961, The magnetic properties of ilmenite–hematite crystals: Royal Soc. London Proc., v. A263, p. 508-530.

Choudhuri, A., and Winkler, H. G. F., 1967, Anthophyllit und Hornblende in einigen metamorphen Reaktionen: Contr. Mineralogy Petrology, v. 14, p. 367-374.

Cooper, A. F., and Lovering, J. F., 1970, Greenschist amphiboles from Haast River, New Zealand: Contr. Mineralogy Petrology, v. 27, p. 11-24.

Czamanske, G. K., and Wones, D. R., 1973, Oxidation during magmatic differentiation, Finnmarka Complex, Oslo area, Norway: Pt. 2. The mafic silicates: Jour. Petrology, v. 14, p. 349-380.

Deer, W. A., Howie, R. A., and Zussman, J., 1962, Rock Forming Minerals: London, Longmans, Green and Co., 270 p.

———— 1966, An introduction to the rock forming minerals: London, Longmans, Green and Co., 528 p.

Engel, A. E. J., and Engel, C. G., 1962a, Progressive metamorphism of amphibolite, northwest Adirondack Mountains, New York: Boulder, Colo., Geol. Soc. America, Buddington Volume, p. 37-82.

———— 1962b, Hornblendes formed during progressive metamorphism of amphibolites, northwest Adirondack Mountains, New York: Geol. Soc. America Bull., v. 73, p. 1499-1515.

Ernst, W. G., 1966, Synthesis and stability relations of ferrotremolite: Am. Jour. Sci., v. 264, p. 37-65.

———— 1972, Ca-amphibole paragenesis in the Shirataki District, central Shikoku, Japan: Geol. Soc. America Mem. 135, p. 73-94.

Essene, E. J., Bohlen, S. R., and Valley, J. W., 1978, Determination of regional water fugacities in the Adirondacks: Geol. Soc. America Abs. with Programs, v. 10, p. 397-398.

Eugster, H. P., Albee, A. L., Bence, A. E., Thompson, J. B., Jr., and Waldbaum, D. R., 1972, The two phase region and excess mixing properties of paragonite–muscovite crystalline solutions: Jour. Petrology, v. 13, p. 147-149.

Eugster, H. P., and Wones, D. R., 1962, Stability relations of the ferruginous biotite, annite: Jour. Petrology, v. 3, p. 82-125.

Ferry, J. M., ms, 1975, Metamorphism of calcareous sediments in the Waterville-Vassalboro area, South-central Maine: Ph.D. thesis, Harvard Univ., 184 p.

Ferry, J. M., and Spear, F. S., 1978, Experimental calibration of the partitioning of Fe and Mg between biotite and garnet: Contr. Mineralogy Petrology, v. 66, p. 113-117.

Gilbert, C. M., 1966, Synthesis and stability relations of the hornblende ferropargasite: Am. Jour. Sci., v. 264, p. 698-742.

Helz, R. T., 1973, Phase relations of basalts in their melting range at P_{H_2O}-5 kb as a function of oxygen fugacity, Part I. Mafic phases: Jour. Petrology, v. 14, p. 249-302.

Hollister, L. S., and Burruss, R. C., 1976, Phase equilibria in fluid inclusions from the Khtada Lake metamorphic complex: Geochim. et Cosmochim. Acta, v. 40, p. 163-175.

Holloway, John, and Burnham, C. W., 1972, Melting relations of basalts with equilibrium H_2O pressure less than total pressure: Jour. Petrology, v. 13, p. 1-29.

Laird, J., ms, 1977, Phase equilibrium of mafic schist and the polymetamorphic history of Vermont: Ph.D. thesis, California Inst. Technology, 445 p.

Leake, B. E., 1965, The relationship between composition of calciferous amphibole and grade of metamorphism, *in* Pitcher, W. S., and Flinn, G. W., eds., Controls of Metamorphism: New York, John Wiley & Sons, p. 299-318.

Lewis, G. N., and Randall, M., 1961, Thermodynamics: New York, McGraw-Hill, 723 p.

Lindsley, D. H., 1973, Delimination of the hematite–ilmenite miscibility gap: Geol. Soc. America Bull., v. 84, p. 657-662.

Liou, J. G., Kuniyoshi, S., and Ito, K., 1974, Experimental studies of the phase relations between greenschist and amphibolite in a basaltic system: Am. Jour. Sci., v. 274, p. 613-632.

Melson, W. G., and Thompson, G., 1973, Glassy abyssal basalts, Atlantic sea floor near St. Paul's Rocks: Petrography and composition of secondary clay minerals: Geol. Soc. America Bull., v. 84, p. 703-716.

Miyashiro, A., Shido, F., and Ewing, M., 1969, Diversity and origin of abyssal tholeiite from the mid-Atlantic ridge near 24° and 30° north latitude: Contr. Mineralogy Petrology, v. 23, p. 38-52.

Papike, J. J., Ross, M., and Clark, J. R., 1969, Crystal-chemical characterization of clinoamphiboles based on five new structure refinements: Mineralog. Soc. America Spec. Paper, 2, p. 117-136.

Robinson, P. R., Ross, M., and Jaffe, H., 1971, Composition of the anthophyllite–gedrite series, comparisons of gedrite and hornblende, and the anthophyllite–gedrite solvus: Am. Mineralogist, v. 56, p. 1005-1041.

Shido, F., and Miyashiro, A., 1959, Hornblendes of basic metamorphic rocks: Toyko Univ. Fac. Sci. Jour., sec. II, v. 12, p. 85-102.

Stoddard, E. F., ms, 1976, Granulite facies metamorphism in the Colton-Rainbow Falls area, N.W. Adirondacks, New York: Ph.D. thesis, Univ. California, 289 p.

Stout, J. H., 1972, Phase petrology and mineral chemistry of coexisting amphiboles from Telemark, Norway: Jour. Petrology, v. 13, p. 99-145.

Touret, Jacques, 1971, Le facies granulite en Norveg Meridionale: II Les includions fluides: Lithos, v. 4, p. 423-436.

Turner, F. J., 1968, Metamorphic Petrology: New York, McGraw-Hill, 650 p.

Tuttle, O. F., 1949, Two pressure vessels for silicate-water studies: Geol. Soc. America Bull., v. 60, p. 1727-1729.

Winkler, H. G. F., 1974, Petrogenesis of Metamorphic Rocks: New York, Springer-Verlag, 320 p.

White, E. W., 1964, Microprobe technique for the analysis of multiphase microcrystalline powders: Am. Mineralogist, v. 49, p. 196-197.

Wones, D. R., and Eugster, H. P., 1965, Stability of biotite: experiment, theory, and application: Am. Mineralogist, v. 50, p. 1228-1272.

Yoder, H. S., and Tilley, C. E., 1962, Origin of basalt magmas: an experimental study of natural and synthetic rock systems: Jour. Petrology, v. 3, p. 342-532.